

Energetics and Dynamics of the Low-Lying Electronic States of Constrained Polyenes: Implications for Infinite Polyenes

Ronald L. Christensen,^{*,†} Miriam M. Enriquez,^{‡,#} Nicole L. Wagner,^{§,#} Alexandra Y. Peacock-Villada,[†] Corina Scriban,^{||} Richard R. Schrock,^{||} Tomáš Polívka,[⊥] Harry A. Frank,^{*,‡} and Robert R. Birge^{*,‡,§}

[†]Department of Chemistry, Bowdoin College, Brunswick, Maine 04011, United States

[‡]Department of Chemistry, University of Connecticut, Storrs, Connecticut 06269-3060, United States

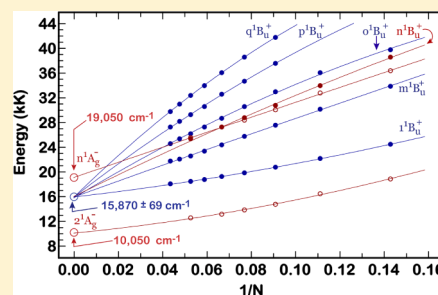
[§]Department of Molecular & Cell Biology, University of Connecticut, Storrs, Connecticut 06269-3125, United States

^{||}Department of Chemistry, Massachusetts Institute of Technology, Cambridge, Massachusetts 02139, United States

[⊥]Institute of Physics and Biophysics, Faculty of Science, University of South Bohemia, České Budějovice, Czech Republic

Supporting Information

ABSTRACT: Steady-state and ultrafast transient absorption spectra were obtained for a series of conformationally constrained, isomerically pure polyenes with 5–23 conjugated double bonds (N). These data and fluorescence spectra of the shorter polyenes reveal the N dependence of the energies of six ${}^1B_u^+$ and two ${}^1A_g^-$ excited states. The ${}^1B_u^+$ states converge to a common infinite polyene limit of $15\,900 \pm 100 \text{ cm}^{-1}$. The two excited ${}^1A_g^-$ states, however, exhibit a large ($\sim 9000 \text{ cm}^{-1}$) energy difference in the infinite polyene limit, in contrast to the common value previously predicted by theory. EOM-CCSD ab initio and MNDO-PSDCI semiempirical MO theories account for the experimental transition energies and intensities. The complex, multistep dynamics of the ${}^1B_u^+ \rightarrow 2^1A_g^- \rightarrow 1^1A_g^-$ excited state decay pathways as a function of N are compared with kinetic data from several natural and synthetic carotenoids. Distinctive transient absorption signals in the visible region, previously identified with S^* states in carotenoids, also are observed for the longer polyenes. Analysis of the lifetimes of the $2^1A_g^-$ states, using the energy gap law for nonradiative decay, reveals remarkable similarities in the N dependence of the $2^1A_g^-$ decay kinetics of the carotenoid and polyene systems. These findings are important for understanding the mechanisms by which carotenoids carry out their roles as light-harvesting molecules and photoprotective agents in biological systems.



1. INTRODUCTION

The discovery of the low-lying $2^1A_g^-$ state in all-*trans* diphenyloctatetraene by Hudson and Kohler¹ in 1972 resulted in a fundamental revision of our understanding of the photophysics and photochemistries of conjugated systems with alternating single and double bonds.^{2,3} In the intervening 40 years, the $2^1A_g^-$ state has been identified and characterized in a large number of polyenes and biologically relevant carotenoids.^{4–7} The seminal discovery of this state and subsequent work on other short, model polyenes was based on the analysis of fluorescence spectra obtained under conditions that provided sufficient vibronic resolution to identify the ${}^1A_g^- \leftrightarrow 2^1A_g^-$ electronic origins. For shorter polyenes, this transition exhibits a characteristic (~ 3000 – 4000 cm^{-1}) Stokes shift relative to the electronic origin of the symmetry-allowed, ${}^1A_g^- \rightarrow {}^1B_u^+$ absorption, which is predicted to be the lowest energy singlet–singlet $\pi\pi^*$ transition (HOMO \rightarrow LUMO) in simple versions of molecular orbital (MO) theory. Theoretical explanations by Schulten, Karplus, and others^{8,9} for $E(2^1A_g^-) < E({}^1B_u^+)$ in all-*trans* polyenes indicated that interactions between the singly and doubly excited electronic configurations were required to account for electron correlation in these extended, one-dimensional π -

electron systems. It also should be noted that the $E(2^1A_g^-) < E({}^1B_u^+)$ state ordering applies to all polyenes with more than three conjugated double bonds.¹⁰

The initial experiments on diphenyloctatetraene¹ and other model, all-*trans* tetraenes,¹¹ pentaenes,¹² and hexaenes¹³ depended on their relatively large, $2^1A_g^- \rightarrow {}^1A_g^-$ fluorescence yields and the ability of these simple systems to be incorporated into low-temperature mixed crystals (typically *n*-alkanes) and glasses. The spectral resolution achieved under these conditions allowed site-selective excitation of polyenes in homogeneous solvent environments and showed that the forbidden ${}^1A_g^- \leftrightarrow 2^1A_g^-$ transitions were made allowed by Herzberg–Teller coupling involving low-frequency ($\sim 100 \text{ cm}^{-1}$) b_u promoting modes.¹⁴ These one-photon optical experiments were followed by investigations of the two-photon-induced fluorescence excitation spectra of octatetraene in low-temperature mixed crystals,^{15,16} which preserve the center of symmetry. These studies verified the assignment of the lowest excited singlet state as $2^1A_g^-$. Subsequently, simple methyl-substituted and

Received: October 25, 2012

Revised: January 16, 2013

Published: January 18, 2013



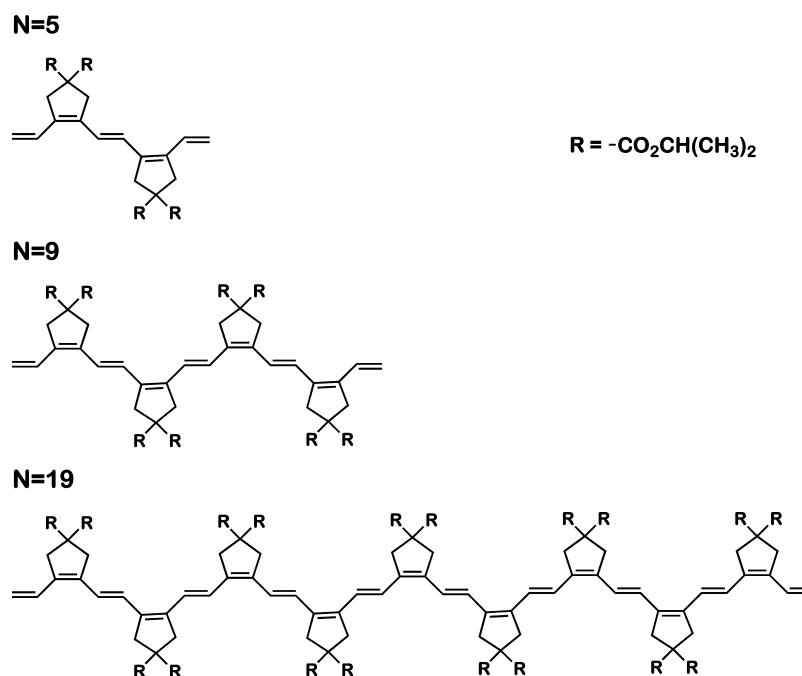


Figure 1. Representative polyene structures.

unsubstituted tetraenes and pentaenes were studied as isolated molecules in supersonic jets, both in one-photon and two-photon fluorescence excitation experiments.^{17–20} This confirmed the earlier assignments of electronic origins and vibronic bands and the influence of symmetry on the intensities of the forbidden transitions. Analysis of the experiments on isolated tetraenes also showed that the oscillator strength for the Herzberg–Teller-allowed $1^1A_g^- \rightarrow 2^1A_g^-$ transition in all-*trans* octatetraene was comparable to the oscillator strength of this transition in *cis* isomers lacking a center of symmetry.^{17–19}

The early studies of the $2^1A_g^-$ state in simple model polyenes later were extended to polyenes of photobiological interest. These include the retinyl chromophores involved in vision^{21,22} and carotenoids employed for light-harvesting and photoprotection in photosynthetic organisms.²³ The functioning of the photosynthetic apparatus depends on the energies and dynamics of the low-energy excited electronic states of the carotenoids and chlorophylls in antenna and reaction center pigment–protein complexes. Initial studies of the $2^1A_g^-$ states in carotenoids having relatively long π -electron conjugated chain lengths relied on the detection of fluorescence signals from the $2^1A_g^-$ state, which become vanishingly small with increasing N . For example, the $2^1A_g^- \rightarrow 1^1A_g^-$ fluorescence yield for all-*trans* β -carotene ($N = 11$) is $\leq 10^{-5}$.^{24,25} This makes the detection and assignment of fluorescence signals quite challenging, particularly because of the crossover to stronger $1^1B_u^+ \rightarrow 1^1A_g^-$ emissions in longer polyenes and carotenoids.²⁶ These higher energy emissions mask the inherently weak, lower energy fluorescence signals from the $2^1A_g^-$ state.

The difficulties in obtaining reliable $2^1A_g^-$ energies for carotenoids were addressed by the development of transient absorption techniques, which demonstrated the feasibility of detecting vibronically resolved, symmetry-allowed $2^1A_g^- \rightarrow 1^1B_u^+$ transitions of carotenoids in the near-infrared (NIR) region.^{27,28} The energy of the $2^1A_g^-$ state then can be calculated from the difference between the $1^1A_g^- \rightarrow 1^1B_u^+$ and $2^1A_g^- \rightarrow 1^1B_u^+$ vibronic origins. Both of these transitions are symmetry-

allowed and relatively strong for all-*trans* isomers. The critical advantages of using transient absorption to determine the $2^1A_g^-$ energies of longer polyenes and carotenoids were reinforced by our recent work on the fluorescence of all-*trans* hexadecaheptaene ($N = 7$).²⁹ These studies indicated that electronic excitation of the all-*trans* species produced distorted, more-highly emissive *trans* structures and *cis* isomers in the $2^1A_g^-$ state and that the $2^1A_g^- \rightarrow 1^1A_g^-$ emission could not be identified with the same distribution of polyene geometries present in the ground state. Thus, earlier reports of fluorescence from longer all-*trans* polyenes and carotenoids must be attributed to more strongly allowed radiative decay from less-symmetric molecules, either present as photochemical impurities, or as distorted ground state conformers, or formed on the $2^1A_g^-$ potential surface following excitation of more-symmetric, all-*trans* species. This scenario is supported by the apparently larger oscillator strengths in longer polyenes ($N > 4$) for $2^1A_g^- \rightarrow 1^1A_g^-$ radiative decay from *cis* isomers and distorted *trans* isomers relative to the symmetry-forbidden transitions of molecules that retain C_{2h} geometry and selection rules.^{2,30}

The advantages of transient absorption measurements here are combined with recent developments in synthetic techniques,^{31,32} which have provided a series of stable, rigid polyenes containing five-membered rings (Figure 1). The peripheral ester groups enhance the solubility of these molecules in a variety of organic solvents without perturbing the interior π orbitals. These molecules have planar π -electron frameworks and are resistant to conformational disorder and thermal and photochemical isomerization. This results in a more homogeneous distribution of ground and excited state geometries, giving well-resolved absorption spectra, even in room temperature solutions.

We have carried out a systematic investigation of the electronic spectroscopy of this homologous series of polyenes, obtaining steady-state absorption spectra in the ultraviolet and visible for $N = 5$ –23 and transient absorption spectra in the

visible and NIR for $N = 7-19$. This has allowed the analysis of an unusually rich set of data to understand the changes in the energies and dynamics of several excited electronic states as a function of N . These experiments provide insights on the photophysics of related polyenes, including carotenoids employed in photobiology. The data also allow comparisons with theoretical predictions of the excited state properties of these molecules in the infinite polyene limit.

The molecules investigated here alternate between C_{2h} and C_{2v} symmetry, sharing a concise Abelian C_2 subgroup. Because the properties of the $\pi\pi^*$ excited states are determined by the C_2 subgroup, which is maintained by all of these polyenes, we can provide an unambiguous discussion of the excited states by referring only to the C_{2h} point group. An extended point group correlation table for the C_{2h} and C_{2v} point groups is provided in the Supporting Information section (Table S1). This approach allows a comparison of the present results with numerous experimental and theoretical studies on linear polyenes² and on a wide range of less symmetrical carotenoids^{23,26,33} and retinyl^{21,22,34} polyenes. We also designate ionic (+) versus covalent (-) states following the work of Schulten, Karplus, and co-workers.^{8,9,35} Linear polyenes with all-*trans* conformations have allowed ${}^1A_g^- \rightarrow {}^1B_u^+$ transitions, and the transitions from the ${}^1A_g^-$ state to all other states (${}^1B_u^-$, ${}^1A_g^+$, and ${}^1A_g^-$) are symmetry forbidden or orbital parity forbidden. *cis*-Linkages induce oscillator strength in transitions to excited ${}^1A_g^+$ states, conventionally designated as *cis* bands. Polar polyenes can induce mixing of the ionic and covalent states, and transitions to the ${}^1B_u^-$ and ${}^1A_g^-$ states can gain oscillator strength, depending upon the direction and magnitude of their dipole moments.^{36,37}

2. MATERIALS AND METHODS

2.1. Sample Purification. Polyenes were synthesized as described previously³² and were received as dried samples. Prior to spectroscopic measurements, samples were purified using a Millipore Waters 600E high-performance liquid chromatography (HPLC) system equipped with a Waters 2996 single diode-array detector. Each polyene was dissolved in methylene chloride and filtered prior to injection into a Phenomenex Ultracarb C18 column (250×4.6 mm, $5 \mu\text{m}$ particle size). The HPLC mobile phase was changed as a linear gradient from acetonitrile/methanol/water (42:53:5, v/v/v) to acetonitrile/methanol (30:70, v/v) over 50 or 60 min at a flow rate of 1 mL/min. The purified samples were collected upon elution from the HPLC, dried under a gentle stream of nitrogen gas, and stored at -80°C until the spectroscopic measurements.

2.2. Steady-State Absorption and Fluorescence Spectroscopy. Absorption spectra in room temperature and 77 K 2-methyltetrahydrofuran (2-MTHF) were recorded on a Cary 400 spectrometer. Spectra at 77 K were obtained from samples slowly frozen in a 1 cm Suprasil cryogenic cuvette (NSG) suspended in a copper holder within a customized flat-windowed (Suprasil) liquid-nitrogen cryostat (Ace Glass). The liquid nitrogen was in contact with the bottom of the copper cuvette holder but did not reach the optical path in the center of the frozen sample. The low-temperature absorption spectra were corrected for the absorption and light scattering of the 2-MTHF glass and other optical components. Fluorescence and fluorescence excitation spectra were obtained on a SPEX/JY Model 212 spectrofluorimeter. All emission spectra were corrected for the wavelength dependence of the photo-

multiplier and other optical components using a correction file traceable to NIST standard lamps. Fluorescence spectra were subjected to mild smoothing (using Savitsky-Golay algorithms^{38,39} implemented by Grams AI software) to reduce the noise inherent in these weakly emitting systems. The smoothing procedures only minimally distorted the relatively broad vibronic details in the emission spectra. In converting fluorescence spectra from wavelength to energy (cm^{-1}) scales, spectra were corrected for the differences between band-passes at constant wavelength resolution vs constant wavenumber resolution, i.e., $I(\tilde{\nu})/d\tilde{\nu} = \lambda^2 I(\lambda)/d\lambda$.⁴⁰ Positions of the vibronic bands were determined by fitting the spectra to sums of Gaussians using Grams AI spectroscopy software. Peak positions of prominent bands were calculated as averages from a range of fits using different numbers of Gaussians and different initial guesses for the least-squares fits.

2.3. Time-Resolved Absorption Spectroscopy. Time-resolved absorption spectra of the polyenes dissolved in 2-MTHF were recorded at room temperature using the femtosecond transient absorption spectrometer system previously described.⁴¹ The laser system consisted of an amplified Ti:sapphire tunable laser (Spectra-Physics Spitfire/Tsunami/Millenia) pumped at a 1 kHz repetition rate by an Evolution 15, Q-switched Nd:YLF laser (Coherent). A Spectra-Physics OPA-800C optical parametric amplifier produced a pump beam with a duration of ~ 60 fs, and a 3 mm Sapphire plate contained in a Helios time-resolved spectrometer (Ultrafast Systems, LLC) generated a white light continuum for probing transients in the visible and NIR spectral regions. Mutual polarization of the pump and probe beams was set at the magic angle (54.7°). The pump wavelengths used in the measurements are specified in Table 1. The pump beam had a diameter of 1 mm and an energy of $\sim 1 \mu\text{J}$ /pulse, resulting in a pump intensity of 2.6 to 3.3×10^{14} photons/ cm^2 pulse. Transient absorption spectra were recorded from samples having absorbances (A) at the excitation wavelength between 0.4 and 0.6 in a 2 mm path length cell. The signals were averaged over 5 s, and the samples were stirred with a magnetic microstirrer to minimize photodegradation. To evaluate the integrity of the samples, steady-state absorption spectra were recorded before and after each transient absorption experiment. Surface Explorer Pro v1.1.5 (Ultrafast Systems, LLC) software was used for chirp correction and to subtract scattered excitation light. Global fitting analysis of the transient absorption spectral and temporal data sets was based on a sequential decay model⁴² and carried out using a modified version of ASUFit v 3.0 software provided by Dr. Evaldas Katilius of Arizona State University. The number of kinetic components required was determined by a chi squared (χ^2) test and by examination of the goodness of fit of the transient decay traces across the entire bandwidth of the spectral profiles.

2.4. Theoretical Analysis. Excited state calculations were carried out using a variety of MO methods for comparative purposes. Modified neglect of differential overlap with partial single- and double-configuration interaction (MNDO-PSDCI) methods^{6,43} were used to study the impact of conformational degrees of freedom on the excited states of all the polyenes. This semiempirical method includes single and double excitations within the π system and has been useful in understanding the electronic properties of short- and long-chain polyenes and carotenoids.^{30,44,45} The standard Austin Model 1 (AM1) parametrization was used: Mataga repulsion integrals ($r_{ijm} = 2$) and identical π and σ electron mobility

constants of 1.7 ($pimc = sigmc = 1.7$).^{6,43} When the π system provided more than ten filled molecular orbitals, the single and double configuration interactions (CISD) were limited to the ten highest energy filled and ten lowest energy virtual π molecular orbitals. Ab initio calculations were carried out by using configuration interaction singles (CIS),⁴⁶ equation of motion coupled cluster with singles and doubles (EOM-CCSD),^{47–49} and symmetry adapted clustered/configuration interaction (SAC-CI)^{50,51} methods as implemented in Gaussian 09.⁵² The CIS calculations were carried out using full single configuration interactions (CI), and the SAC-CI calculations were carried out at highest precision [full single CI and extensive double CI (LevelThree selection)].^{50,53} The active space of the EOM-CCSD calculations was modified for each calculation to include the entire π system minus the highest energy unfilled and lowest energy filled π orbitals. Exclusion of these outer π orbitals had no meaningful impact on the nine lowest energy transitions, and the EOM-CCSD methods are highly efficient and size consistent with appropriate selection of the active space.⁵⁴ Excited state properties were calculated relative to the second order Møller–Plesset (MP2) ground state.⁵⁵ All ab initio calculations used the double- ζ D95 basis set.⁵⁶ CASSCF methods and state averaged optimization methods were used to search for conical intersections in the smaller polyenes, but no such features were found. We examine this issue in more detail in section 3.4.

3. RESULTS AND DISCUSSION

3.1. Absorption and Dynamics of Polyene Excited States in Room Temperature Solutions. 3.1.1. Steady-State Absorption Spectra.

Steady-state absorption spectroscopy of polyenes with $N = 5–23$ lead to the identification of several allowed electronic transitions in these systems.³² The relatively rigid, planar structures of these polyenes result in well-resolved absorption spectra, even in room temperature solutions, as demonstrated for polyenes with $N = 5, 9$, and 19 in Figure 2. The vibronic progressions reflect partially resolved combinations of totally symmetric C–C and C=C stretches, and the strongly allowed, low energy $1^1A_g^- \rightarrow 1^1B_u^+$ transitions exhibit vibronic intervals ranging from $\sim 1500\text{ cm}^{-1}$ for $N = 5$ to $\sim 1200\text{ cm}^{-1}$ for $N = 19$. Analysis of the vibronic bands indicates an almost constant line width of $\sim 1000\text{ cm}^{-1}$,

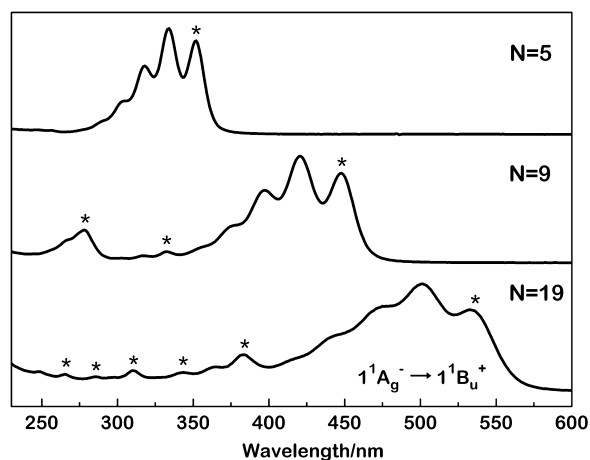


Figure 2. Room temperature, steady-state absorption spectra of $N = 5, 9$, and 19 . Asterisks indicate positions of electronic origins ((0–0) bands) for allowed transitions.

regardless of the energy of the electronic transition or the length of conjugation. The relatively high vibronic resolution in room temperature solutions, combined with our ability to systematically follow the shifts of spectral features as a function of the number of conjugated double bonds, greatly aids the identification and assignments of the origins ((0–0) bands) of the electronic transitions in these systems. Assignments of the weaker, higher energy transitions further are facilitated by their systematically stronger dependence on N . The electronic origins for several electronic transitions for $N = 5, 9$, and 19 are indicated in Figure 2.

3.1.2. Transient Absorption Spectra in the Visible Region.

We recorded ultrafast, time-resolved, transient absorption spectra of polyenes with $N = 7–19$ in room temperature solutions of 2-MTHF. Spectra in the 450–800 nm wavelength region at various delay times between the pump and probe pulses are given in Figure 3. The negative amplitudes observed between 450 and 700 nm correspond to the depletion of the ground state and bleaching of the strongly allowed $1^1A_g^- \rightarrow 1^1B_u^+$ absorption; cf. Figure 2. The positive transient absorption signals between 500 and 800 nm are assigned to a symmetry-allowed $2^1A_g^- \rightarrow n^1B_u^+$ transition.⁵⁷ In parallel with trends observed in the steady-state absorption spectra (Figure 2), all of the transient absorption features show systematic shifts to longer wavelengths with increasing N . Also, it is significant that, for both the steady-state and transient absorption spectra, the relative transition intensities show no detectable differences for molecules with C_{2h} ($N = 5, 9, 13, 17$, and 21) vs C_{2v} ($N = 7, 11, 15, 19$, and 23) symmetries. This supports the use of the C_{2h} symmetry labels and selection rules for describing the electronic spectroscopy of all polyenes in this series.

The components in the transient absorption spectra are revealed by a global fitting analysis of the spectral and temporal data sets according to a sequential decay model, yielding “Evolution Associated Difference Spectra” (EADS), which also are shown in Figure 3 for $N = 7–19$. The lifetimes of the kinetic components are given in Table 1. Note that for $N = 7–15$ (Table 1), three EADS components are needed to account for the transient absorption signals in the 450–800 nm range. $N = 19$ requires a fourth EADS component for a good fit. For all molecules, the shortest lived of these components occurs between 90 and 180 fs and can be assigned to a combination of the bleaching of the $1^1A_g^- \rightarrow 1^1B_u^+$ transition ($\lambda \approx 450–550\text{ nm}$) and $1^1B_u^+ \rightarrow 1^1A_g^-$ stimulated emission (weak negative signals with $\lambda \approx 550–700\text{ nm}$). These fast decays are typical of the $1^1B_u^+$ lifetimes of related carotenoids.^{57–59} Although the instrument response time of $\sim 100\text{ fs}$ precludes a more quantitative analysis, the $1^1B_u^+$ lifetime clearly decreases with increasing N , as previously noted for carotenoids.⁶⁰

For $N = 7, 9$, and 11 , the second EADS component obtained from a fit to the transient absorption data in the visible region (Figure 3) has a lifetime (τ_1') of 500–1000 fs (Table 1) and can be identified with the decay of a symmetry-allowed, $2^1A_g^- \rightarrow n^1B_u^+$ transition from a vibronically excited $2^1A_g^-$ electronic state. Similar EADS components have been assigned as hot bands in the $2^1A_g^- \rightarrow n^1B_u^+$ transitions of carotenoids,^{57,61,62} indicating relatively slow vibrational relaxation within the $2^1A_g^-$ states. For the shorter polyenes ($N = 7–11$), this spectral feature is displaced by $\sim 1800\text{ cm}^{-1}$ from the (0–0) band associated with the $2^1A_g^- \rightarrow n^1B_u^+$ transitions from vibrationally relaxed $2^1A_g^-$ states. These vibronic spacings are consistent with significant increases in $2^1A_g^-$ of the frequencies of the totally symmetric (a_g) C=C stretching modes that dominate

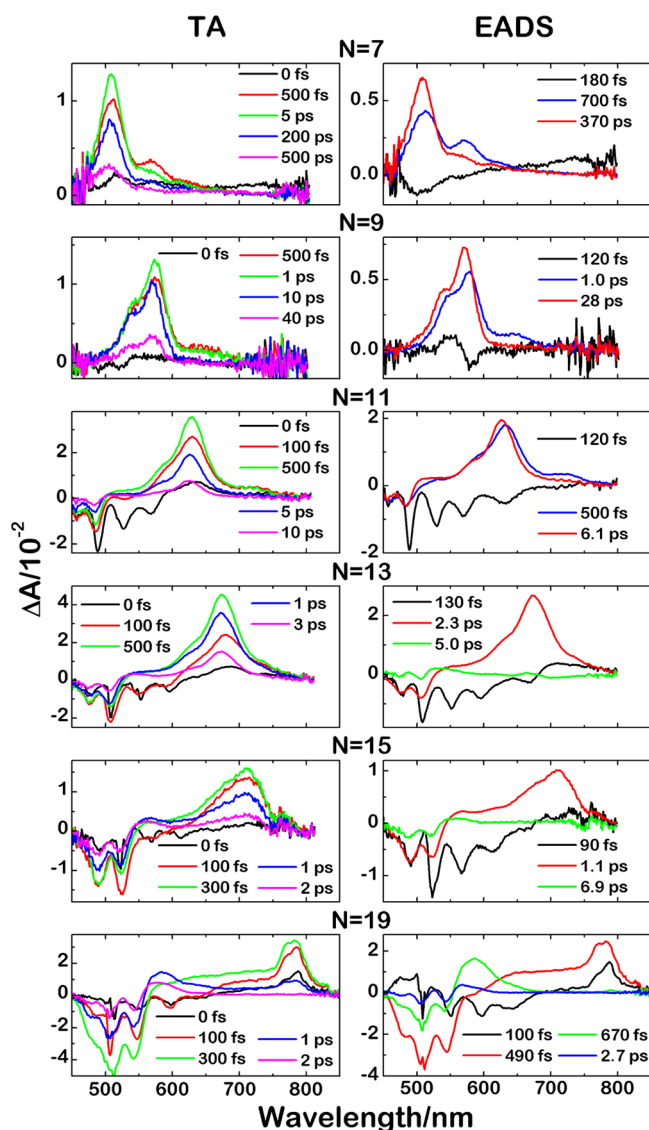


Figure 3. Transient absorption (TA) spectra obtained at different time delays in the visible at room temperature in 2-MTHF. Global analysis of decays provides evolution associated difference spectra (EADS).

polyene electronic spectra, cf. vibronic spacings of $\sim 1400\text{ cm}^{-1}$ for the $1^1A_g^- \rightarrow 1^1B_u^+$ transitions of $N = 7-11$ (Figure 2). This increase, first noted in high-resolution optical spectra of model pentaenes and hexaenes,¹²⁻¹⁴ is due to vibronic coupling between the $1^1A_g^-$ and $2^1A_g^-$ states. Similar increases have been observed in a variety of carotenoids.^{57,61,62}

Table 1. Lifetimes of the Relaxed $2^1A_g^-$ (τ_1), Vibrational Hot $2^1A_g^-$ (τ'_1), $1^1B_u^+$ (τ_2), and Other Components from Global Fitting of the Transient Absorption Spectra

N	λ_{ex} (nm)	τ_1 (ps) ^a	τ'_1 (ps)	τ_2 (fs) ^b	τ_3 (ps)
7	410	$370 \pm 10/340 \pm 50$	0.7 ± 0.1	$180 \pm 40/160 \pm 40$	
9	400	$28 \pm 3/28 \pm 5$	1.0 ± 0.3	$120 \pm 30/150 \pm 10$	
11	490	$6.1 \pm 0.3/5.3 \pm 1.0$	0.5 ± 0.1	$120 \pm 50/140 \pm 10$	
13	508	$2.3 \pm 0.2/2.6 \pm 0.5$		$130 \pm 30/100 \pm 30$	5.0 ± 0.5
15	517	$1.1 \pm 0.2/1.2 \pm 0.1$		$90 \pm 10/70 \pm 10$	6.9 ± 0.5
19	508	$0.49 \pm 0.01/0.50 \pm 0.05$		$100 \pm 10/70 \pm 10$	0.67 ± 0.03 2.7 ± 0.2

^a $2^1A_g^-$ lifetimes derived from visible/NIR transient absorption spectra. ^b $1^1B_u^+$ lifetimes derived from visible/NIR transient absorption spectra.

Polyenes with $N = 13, 15,$ and 19 lack kinetic features associated with an intermediate, vibronically hot $2^1A_g^-$ component, and for these molecules, the second EADS component can be assigned to the decay of thermally equilibrated $2^1A_g^-$ (S_1) states. It should be noted that, even for $N = 7, 9,$ and 11 , the spectral features associated with vibrational relaxation in $2^1A_g^-$ are significantly weaker than those observed for carotenoids,^{57,63} most likely due to the relative rigidity of these systems. The small amplitude EADS components in the shorter polyenes, identified with $2^1A_g^-$ vibrational relaxation, may be due to larger geometry changes (and larger Franck–Condon factors) when the smaller molecules are excited into their $1^1B_u^+$ and $2^1A_g^-$ states. This would give rise to larger transient populations of vibrational states involving C–C and C=C stretches. For $N = 7, 9,$ and 11 , the lifetime of the vibrationally relaxed $2^1A_g^-$ state (τ_1) decreases from 370 to 28 ps. The trend continues for $N = 13, 15,$ and 19 (second EADS components), with $2^1A_g^-$ lifetimes (τ_1) of 2.3, 1.1, and 0.49 ps, respectively (Table 1). We note that the $2^1A_g^-$ lifetimes for this series primarily reflect the rates of nonradiative decay since, for long ($N \geq 7$) polyenes, the radiative decay rates for the symmetry-forbidden $2^1A_g^- \rightarrow 1^1A_g^-$ transitions ($\leq 10^7/\text{s}$) are much smaller than the rates of nonradiative relaxation.^{64,65} As will be discussed in section 3.4, the $2^1A_g^-$ lifetimes can be related to the systematic decrease in the energy of the $2^1A_g^-$ state with increasing conjugation length, following the energy gap law for radiationless decay.^{57,66}

The transient absorption spectra and EADS components of these constrained polyenes are remarkably similar to those of a wide variety of less rigid, less symmetric, biologically relevant carotenoids.^{45,57,59,67-70} These similarities include the presence of longer decay components, observed exclusively in polyenes with $N = 13, 15,$ and 19 , which are particularly prominent for $N = 19$. These components (the third EADS with lifetimes of 5.0, 6.9, and 2.7 ps for $N = 13, 15,$ and 19) have weak absorptions on the blue side of the main $2^1A_g^- \rightarrow n^1B_u^+$ absorption band. Following previous discussions of the transient absorption spectra of longer carotenoids such as spirilloxanthin ($N = 13$),⁵⁷ these features are assigned to what have been labeled as S^* states. In $N = 19$, there is a fourth EADS component with $\tau = 0.67$ ps (Figure 3 and Table 1) with a spectrum similar to that of the S^* state, suggesting that multiple S^* signals may be present in the longest polyene. This also is consistent with what has been reported for long carotenoids.⁵⁷

The S^* state has been the subject of significant discussion and controversy.⁷¹ An early explanation for the S^* signals, first reported for a β -carotene analogue with $N = 19$, was that they were due to $1^1A_g^- \rightarrow 1^1B_u^+$ absorptions from vibrationally

excited $1^1A_g^-$ states,²⁵ which later were attributed to population by impulsive stimulated Raman scattering (ISRS) during the excitation pulse.⁶⁹ The complexity of interpreting S^* signals for a wide range of carotenoids and the current polyenes is illustrated by recent work on β -carotene. The ISRS hypothesis was explored by Jailaubekov et al.,⁷² who compared narrow and broad band excitation of room temperature β -carotene solutions and demonstrated that even excitation with narrow band pulses generated the S^* signal, ruling out the ISRS mechanism. Lenzer et al.⁷³ consequently assigned the S^* features in β -carotene in *n*-hexane as absorption from vibrationally excited $1^1A_g^-$, directly populated via internal conversion from $2^1A_g^-$, as originally proposed by Gillbro et al.²⁵ However, these conclusions have been challenged by recent broad band 2D electronic spectroscopy of β -carotene in a 77 K glass,⁷⁴ which demonstrated that ISRS can be important when conformational flexibility is limited. Similar geometric restrictions may apply to these constrained polyenes, even in room temperature solutions.

One of several competing explanations associates S^* with distorted or twisted conformers on the $2^1A_g^-$ potential surface, populated via $1^1B_u^+$.^{45,67} For example, for ground state spirilloxanthin ($N = 13$), torsional motions around the single and double bonds have been proposed to lead to a more compact, corkscrew structure with a small dipole moment, which stabilizes the interactions of the $1^1A_g^-$ state with the solvent. Excitation into the $2^1A_g^-$ state can unravel this corkscrew geometry, leading to additional channels for relaxation and potentially complex, time-dependent signals associated with absorption from $2^1A_g^-$.⁵⁷ The presence of S^* signals in $N = 13$ and $N = 15$ (Figure 3) suggests a similar explanation, though it is important to emphasize that the ground and excited states of these relatively planar and highly constrained polyenes offer a much more restricted set of twisting coordinates than those available to carotenoids.⁵⁷ These polyenes cannot undergo large amplitude motions and have a more limited number of conformational minima on the $1^1A_g^-$ and $2^1A_g^-$ potential surfaces. For example, under the same thermal and photochemical conditions that convert all-*trans* β -carotene ($N = 11$) into equilibrium mixtures of *cis* and *trans* isomers, the corresponding $N = 11$ polyene in this series is essentially unreactive.⁷⁵ The observation of relatively strong and characteristic S^* signals in these geometrically constrained polyenes thus significantly narrows the range of motions required to account for similar transient absorption signals in the carotenoids.

Another important observation regarding the origin of the S^* signals is the excited state dynamics of the $N = 19$ polyene. Analysis of the transient absorption spectra shown in Figure 3 (bottom right panel) shows that the second EADS component (red) exhibits strong $2^1A_g^- \rightarrow n^1B_u^+$ absorption at 780 nm but no S^* signals. This absorption decays in 490 fs to form a third EADS component (green) with relatively strong S^* signals at 580 nm. As shown in Figure S1, Supporting Information, the rise times of the S^* signals in $N = 19$ equal the decay time of the $2^1A_g^-$ state, indicating that S^* is directly populated from $2^1A_g^-$. These kinetics have not been seen in previous studies of carotenoids and suggest that the $N = 19$ S^* signals are due to $1^1A_g^- \rightarrow 1^1B_u^+$ absorption from excited vibrational levels of the ground state ($1^1A_g^-$), as previously suggested for β -carotene.⁷³ However, this model cannot explain the dynamics of the $N = 13$ and $N = 15$ polyenes or the S^* signals in spirilloxanthin ($N = 13$) or rhodoxanthin ($N = 14$).^{76–78} For all of these molecules, S^*

signals appear within 200–500 fs, well in advance of the >1 ps decay times of the $2^1A_g^-$ states. (See the transient absorption traces for $N = 13$ and 15 in Figure 3.) The 490 fs component in $N = 19$ also might be explained by S^* as a twisted $2^1A_g^-$ excited state that is generated within the 490 fs $2^1A_g^-$ lifetime. Additional experimental and theoretical studies of the dynamics of this constrained polyene series ($N = 5–23$) promise to provide further insights on the role of molecular structure, conjugation length, and the ultrafast excitation conditions on the S^* signals in a wide range of polyenes and carotenoids in different solvent environments. However, further refinement and integration of the different models for the S^* signals remain to be significant challenges and fall outside the scope of this article.

3.1.3. Transient Absorption Spectra in the NIR Region. Time-resolved, transient absorption spectra of the $N = 7–19$ polyenes in the NIR ($\sim 850–1400$ nm) in room temperature 2-MTHF are given in Figure 4. These signals can be accounted for by two EADS components as indicated. The short-lived (70–160 fs, cf. ~ 100 fs instrument response) components in

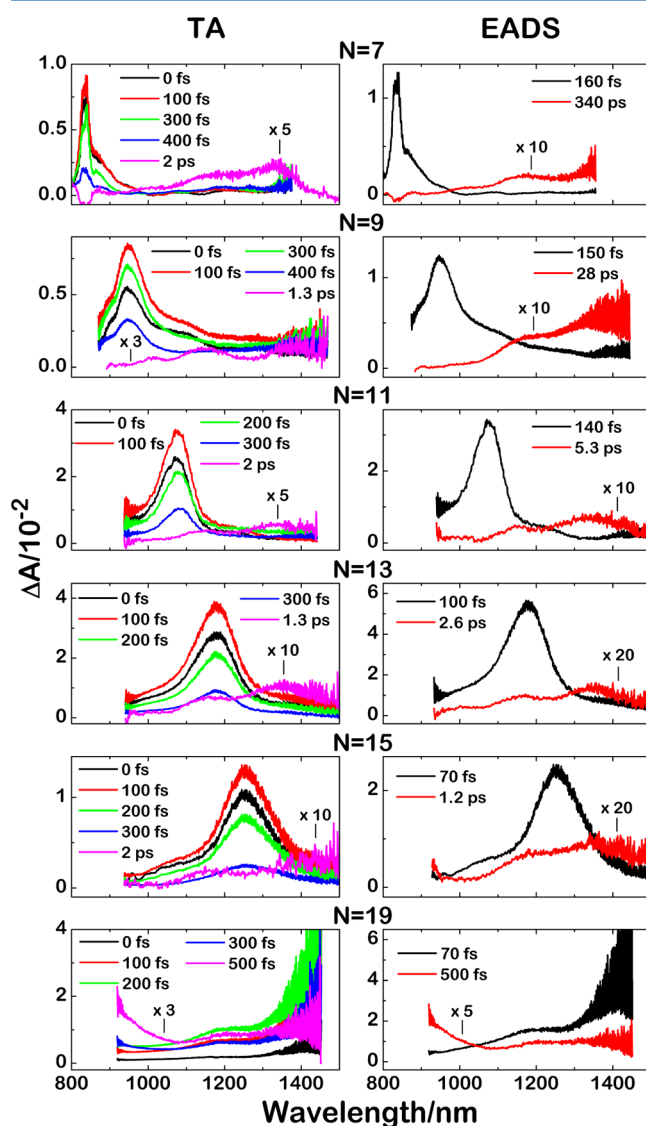


Figure 4. Transient absorption (TA) spectra obtained at different time delays in the NIR at room temperature in 2-MTHF. Global analysis of decays provides evolution associated difference spectra (EADS).

the NIR transient absorptions can be identified with a symmetry-allowed, $1^1B_u^+ \rightarrow n^1A_g^-$ absorption. As expected, these transitions show a systematic shift to longer wavelength with increasing conjugation (~ 840 nm for $N = 7$; ~ 1400 nm for $N = 19$). The lifetimes of these components are in good agreement with the $1^1B_u^+$ lifetimes (90–180 fs) from the EADS analysis of the transient absorption spectra in the visible region (Table 1). The energies of $1^1A_g^- \rightarrow 1^1B_u^+$ (0–0) bands can be added to the $1^1B_u^+ \rightarrow n^1A_g^-$ transition energies to calculate the energy of the $n^1A_g^-$ state as a function of conjugation length. The transient absorption experiments thus provide detailed data on a second, higher energy dark state, which cannot be detected in the steady-state absorption spectra (Figure 2).

The NIR spectra also lead to the determination of the energies of the lowest energy single state ($2^1A_g^-$). For shorter, model systems ($4 \leq N \leq 7$), the $2^1A_g^-$ state can be observed in fluorescence experiments,^{5,29} but the dominance of non-radiative decay processes makes it difficult to detect $2^1A_g^- \rightarrow 1^1A_g^-$ transitions in longer ($N > 7$) polyenes and carotenoids. It now is clear that previously reported $2^1A_g^- \rightarrow 1^1A_g^-$ fluorescence in all-*trans* carotenoids and long polyenes most likely can be attributed to *cis* impurities and/or conformationally distorted all-*trans* species, either present in distributions of $1^1A_g^-$ geometries or formed on $2^1A_g^-$ potential surfaces.²⁹ The measurement of the energies and dynamics of $2^1A_g^-$ states in carotenoids and polyenes thus is more reliably accomplished by detecting the symmetry-allowed $2^1A_g^- \rightarrow 1^1B_u^+$ transition, as originally demonstrated by Polívka and Sundström.²⁷

The long-lived EADS components shown in Figure 4 display weak $2^1A_g^- \rightarrow 1^1B_u^+$ absorptions in the 1000–1400 nm range, but there is sufficient signal and vibronic resolution to analyze these features and to assign vibronic bands. As with the other electronic transitions in the steady-state and transient absorption spectra, our ability to compare spectra of molecules over a wide range of conjugation lengths is an indispensable tool in assigning the vibronic bands. In addition, previous work on the $2^1A_g^- \rightarrow 1^1B_u^+$ absorptions in a variety of carotenoids is crucial in understanding similar signals in these constrained systems. The lifetimes of the longest-lived EADS components in the NIR are in excellent agreement with those obtained for the much stronger $2^1A_g^- \rightarrow n^1B_u^+$ transitions in the visible region (Table 1). We thus can be assured that the weak absorptions detected in the NIR correspond to transitions from thermally relaxed $2^1A_g^-$ states. No components corresponding to the S^* signals were observed in the NIR, as noted in a previous study on the carotenoid spirilloxanthin.⁷⁹

3.2. Energies of the Low-Lying Electronic States.

3.2.1. Fluorescence Spectroscopy of $N = 5$ and $N = 7$. An understanding of the low-lying $2^1A_g^-$ states in linear polyenes, including carotenoids, initially emerged from analysis of the low temperature absorption and emission spectra of short model systems.^{3,10} Simple all-*trans* polyenes with $N = 4$ –7 have detectable fluorescence and exhibit spectra with sufficient vibronic resolution to allow the identification of the electronic origins and other vibronic bands of the lowest energy singlet to singlet transitions ($1^1A_g^- \rightarrow 1^1B_u^+$ and $2^1A_g^- \rightarrow 1^1A_g^-$).^{5,80} The canonical fluorescence characteristics of polyenes are well illustrated by the $N = 5$ and $N = 7$ members of the current series. However, the rigid, planar geometries of these molecules result in negligible $2^1A_g^- \rightarrow 1^1A_g^-$ ($S_1 \rightarrow S_0$) fluorescence yields for $N > 7$, and we must rely on transient absorption experiments to determine the energies and dynamics of the lowest lying singlet states for polyenes with larger N .

Fortunately, for $N = 7$, we can compare the electronic transition energies obtained from fluorescence spectra ($2^1A_g^- \rightarrow 1^1A_g^-$) with those deduced from transient absorption ($2^1A_g^- \rightarrow 1^1B_u^+$). The overlap of the two complementary techniques for $N = 7$ proved to be crucial in assigning the weak $2^1A_g^- \rightarrow 1^1B_u^+$ vibronic bands in the NIR absorption spectra (Figure 4), allowing the determination of the $2^1A_g^-$ (S_1) energies for polyenes with $N > 7$.

The $N = 5$ polyene displays the signature absorption and fluorescent spectra of short, model polyene systems (Figure 5).

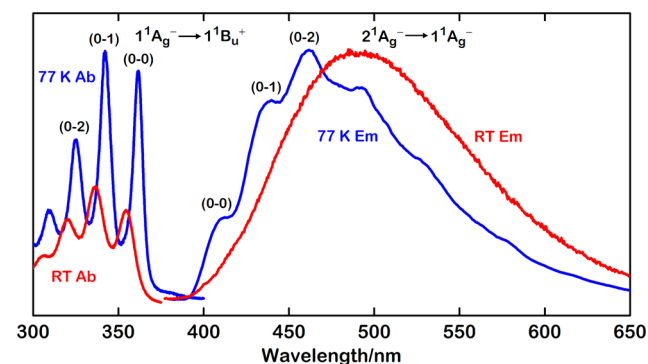


Figure 5. Room temperature and 77 K absorption and fluorescence spectra of $N = 5$ in 2-MTHF. For room temperature emission, $\lambda(\text{excitation}) = 354$ nm; for 77 K emission, $\lambda(\text{excitation}) = 360$ nm.

The room temperature and 77 K absorption spectra ($1^1A_g^- \rightarrow 1^1B_u^+$) both exhibit well-resolved vibronic bands at ~ 1500 cm^{-1} intervals, which can be assigned to overtones and combinations of totally symmetric carbon–carbon single and double bond stretching vibrations. The degree of vibronic resolution in the room temperature absorption spectra suggests a relatively homogeneous distribution of ground state polyene geometries with essentially coplanar, π -conjugated, double, and single bonds. Cooling the sample to 77 K results in a ~ 500 cm^{-1} shift to lower energy of the strongly allowed $1^1A_g^- \rightarrow 1^1B_u^+$ absorption and also results in a significant narrowing of the vibronic bands and a concomitant increase in absorbance. The increase in absorbance and the bathochromic shift in part are due to the increases in solute concentration and the larger refractive index of the higher density, low temperature glass, but the shift to longer wavelengths and the spectral narrowing also can be attributed to an increase in conformational order, resulting in an even narrower distribution of approximately planar molecular geometries.

The $N = 5$ fluorescence spectra exhibit the classic Stokes shift between the strongly allowed ($\epsilon > 10^5$ L/mol cm) absorption ($1^1A_g^- \rightarrow 1^1B_u^+$) and the symmetry-forbidden emission ($2^1A_g^- \rightarrow 1^1A_g^-$). The low temperature emission spectrum has sufficient vibronic resolution to allow the identification of the $2^1A_g^- \rightarrow 1^1A_g^-$ (0–0) band at $24\,450 \pm 20$ cm^{-1} (409 nm), giving a $1^1B_u^+ - 2^1A_g^-$ energy gap of ~ 4800 cm^{-1} at 77 K. These data agree well with the $2^1A_g^-$ (S_1) energies of simpler $N = 5$ polyene hydrocarbons. For example, all-*trans* dodecapentaene has an $2^1A_g^-$ energy of $\sim 24\,200$ cm^{-1} in room temperature, nonpolar hydrocarbon solvents,⁵ which reinforces the observation that the $1^1A_g^- \leftrightarrow 2^1A_g^-$ transition energies of polyenes primarily depend on the conjugation length N and are relatively insensitive to the details of substitution and solvent environment. $1^1A_g^- \leftrightarrow 1^1B_u^+$ transition energies, however, are much more dependent on the molecular structure and solvent,

primarily due to the much larger ($\sim 100\times$) transition dipole of this strongly allowed transition.²⁶

It is important to note that, while the $1^1A_g^- \rightarrow 1^1B_u^+$ absorption of the $N = 5$ polyene shifts to lower energy upon cooling to 77 K, the Franck–Condon envelope of the $2^1A_g^- \rightarrow 1^1A_g^-$ emission shifts to higher energy with cooling (Figure 5). The lack of vibronic resolution in the room temperature emission spectrum makes this shift difficult to quantify, but the combination of the $\sim 500\text{ cm}^{-1}$ red shift in absorption and a comparable blue shift in the emission suggests a substantially larger ($\sim 5800 \pm 300\text{ cm}^{-1}$) $1^1B_u^+ - 2^1A_g^-$ energy gap in the room temperature solution for $N = 5$. The shift of the $2^1A_g^- \rightarrow 1^1A_g^-$ transition to higher energy upon cooling to 77 K can be rationalized by the inability of the relatively short-lived $2^1A_g^-$ state to relax its geometry in the rigid low-temperature glass. There is evidence for similar blue shifts in the $2^1A_g^- \rightarrow 1^1A_g^-$ emissions in several other polyenes. For example, we previously noted increases of $\sim 500\text{ cm}^{-1}$ in the $2^1A_g^- \rightarrow 1^1A_g^-$ (0–0) bands in dimethyl polyenes with $N = 4-7$ upon cooling these molecules from room temperature to 77 K in *n*-alkane solvents.⁸¹ These changes, in combination with the red shifts in the $1^1A_g^- \rightarrow 1^1B_u^+$ absorptions, decrease the $1^1B_u^+ - 2^1A_g^-$ gaps by $\sim 1200\text{ cm}^{-1}$ when these model polyenes are immobilized in 77 K matrixes. A $\sim 500\text{ cm}^{-1}$ red shift of the $1^1A_g^- \rightarrow 1^1B_u^+$ absorption and a $\sim 400\text{ cm}^{-1}$ blue shift of the $2^1A_g^- \rightarrow 1^1A_g^-$ ($S_1 \rightarrow S_0$) emission spectrum upon cooling room temperature samples to 77 K also was observed in a model $N = 7$ open-chain carotenoid,⁶⁴ and comparable blue shifts are noted in the broad, unresolved $S_1 \rightarrow S_0$ ($2^1A_g^- \rightarrow 1^1A_g^-$) emissions of the $N = 7$ and $N = 8$ analogues of β -carotene.⁶⁵

The room temperature and 77 K absorption and fluorescence spectra of $N = 7$ (Figure 6) reveal similar patterns, though the

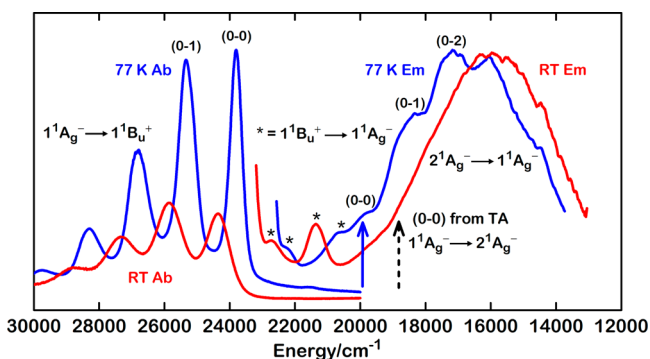


Figure 6. Room temperature and 77 K absorption and fluorescence spectra of $N = 7$ in 2-MTHF. For room temperature emission, $\lambda(\text{excitation}) = 408\text{ nm}$; for 77 K emission, $\lambda(\text{excitation}) = 416\text{ nm}$. The blue and black arrows correspond to the (0–0) bands of $1^1A_g^- \leftrightarrow 2^1A_g^-$ transitions obtained from the 77 K fluorescence spectrum and calculated from the room temperature transient absorption (TA) measurements.

fluorescent yield of $N = 7$ is significantly smaller than that of $N = 5$. The longer polyene exhibits both $1^1B_u^+ \rightarrow 1^1A_g^-$ and $2^1A_g^- \rightarrow 1^1A_g^-$ emissions, and the overlap of these two spectra presents some challenges in assigning the $S_1 \rightarrow S_0$ (0–0) band. Using the $N = 5$ spectra as a guide, we note that the vibronic bands of the well-resolved $1^1A_g^- \rightarrow 1^1B_u^+$ absorption and the $1^1B_u^+ \rightarrow 1^1A_g^-$ emission show parallel shifts ($\sim 500\text{ cm}^{-1}$) to longer wavelengths upon cooling. The $2^1A_g^- \rightarrow 1^1A_g^-$ fluorescence spectrum undergoes a 500–1000 cm^{-1} shift to

shorter wavelengths in the 77 K glass. Using sums of Gaussian fits, the $2^1A_g^- \rightarrow 1^1A_g^-$ vibronic origin for $N = 7$ at 77 K was determined to be $19\,900 \pm 100\text{ cm}^{-1}$ (503 nm). This compares with $19\,600\text{ cm}^{-1}$ for hexadecaheptaene ($N = 7$) in a 77 K EPA glass⁸¹ and $\sim 19\,200\text{ cm}^{-1}$ in various hydrocarbon solvents at room temperature.⁵ These energies also can be compared with a $2^1A_g^-$ energy of $18\,540 \pm 40\text{ cm}^{-1}$ for an $N = 7$ open-chain carotenoid in 77 K EPA.⁶⁴ As for $N = 5$, the $N = 7$ spectra thus show a significant narrowing of the $1^1B_u^+ - 2^1A_g^-$ energy gap when room temperature solutions are frozen into 77 K rigid matrixes. Other important features to note in the $N = 7$ spectra are the characteristic vibronic progressions, which facilitate the precise measurement of the (0–0) transition energies in all but the room temperature fluorescence spectra.

The $N = 9$ polyene has extremely weak fluorescence signals, which are dominated by $1^1B_u^+ \rightarrow 1^1A_g^-$ emission. A crossover from $2^1A_g^- \rightarrow 1^1A_g^-$ ($S_1 \rightarrow S_0$) emission to $1^1B_u^+ \rightarrow 1^1A_g^-$ emission is a common feature of longer polyenes ($N \geq 7$)^{26,82} and precludes the detection of the $2^1A_g^- \rightarrow 1^1A_g^-$ (0–0) band for $N = 9$. Our inability to detect $S_1 \rightarrow S_0$ emission in $N = 9$ is consistent with earlier work on the temperature dependence of the $S_1 \rightarrow S_0$ fluorescence of all-*trans* hexadecaheptaene ($N = 7$),²⁹ which suggested that the previously reported fluorescence from longer polyenes and carotenoids most likely is due to subsets of *cis* impurities and/or higher energy and distorted/twisted all-*trans* species formed in the $2^1A_g^-$ states following excitation of symmetric, all-*trans* molecules. The rigid, planar structures induced by the framework of five-membered rings in the current polyenes preclude large amplitude distortions or *trans* \leftrightarrow *cis* isomerization⁷⁵ and likely result in $1^1A_g^-$ and $2^1A_g^-$ potential surfaces with fewer distorted conformational minima that can be populated in room temperature solutions or 77 K glasses. This can explain the vanishing $2^1A_g^- \rightarrow 1^1A_g^-$ fluorescence signals from these samples compared to their more flexible carotenoid and polyene counterparts with $N > 7$. It is important to stress that, for $N = 7$ of the current polyene series, the comparison of $1^1A_g^- \leftrightarrow 2^1A_g^-$ (0–0) bands estimated from fluorescence and from transient absorption measurements should relate sets of molecules with very similar, relatively homogeneous distributions of ground and excited state geometries.

3.2.2. Assignment of Vibronic Bands in $2^1A_g^- \rightarrow 1^1B_u^+$ Transient Absorption Spectra. Our analysis of the room temperature and 77 K absorption and emission spectra of the $N = 5$ and $N = 7$ polyenes was essential in interpreting the $2^1A_g^- \rightarrow 1^1B_u^+$, NIR transient absorption measurements on $N = 7-19$, which were carried out in room temperature, 2-MTHF solutions. These spectra are presented in Figure 7, along with representative sums of Gaussian fits to spectra obtained from global fitting (EADS). The $2^1A_g^- \rightarrow 1^1B_u^+$ vibronic spacings calculated from the Gaussian fits ($\sim 1450\text{ cm}^{-1}$ for $N = 7$; $\sim 1200\text{ cm}^{-1}$ for $N = 19$) are in good agreement with those observed in the room temperature $1^1A_g^- \rightarrow 1^1B_u^+$ spectra ($\sim 1500\text{ cm}^{-1}$ for $N = 7$; $\sim 1200\text{ cm}^{-1}$ for $N = 19$ (Figure 2)). The dependence of the $1^1B_u^+$ vibronic energies on N parallels the decrease in the frequencies of the $2^1A_g^-$ C–C and C=C vibrational modes with increasing N in *tert*-butyl capped polyenes.⁸³ Sums of Gaussian fits to the raw $2^1A_g^- \rightarrow 1^1B_u^+$ transient absorption data in the NIR are in excellent agreement with fits made to the EADS spectra. The analyses of these fits are greatly simplified by the remarkable consistency of the NIR absorbance features for $N = 7, 9, 11, 13, 15,$ and 19 (Figure 7), which indicates an almost constant $1^1B_u^+ - 2^1A_g^-$ energy

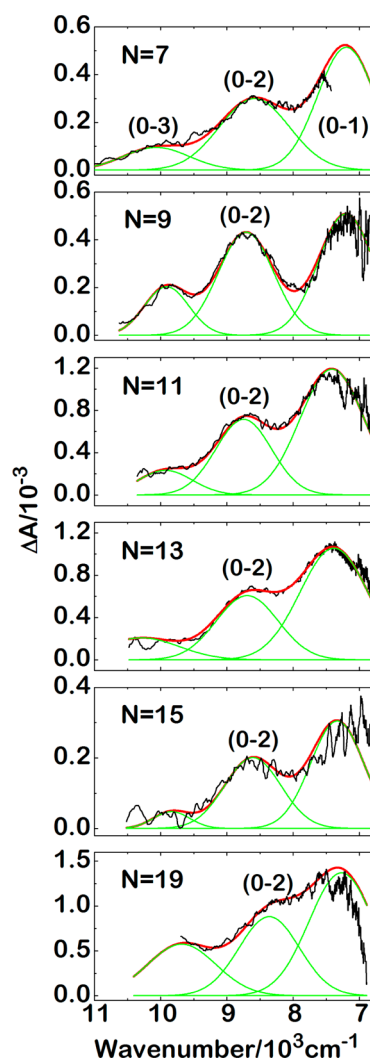


Figure 7. Representative sum of Gaussian fits to NIR transient absorption spectra ($2^1A_g^- \rightarrow 1^1B_u^+$).

difference in this series. Our interpretation of these spectra also builds on previous vibronic analyses of the NIR, $2^1A_g^- \rightarrow 1^1B_u^+$ transient absorption spectra of several carotenoids.^{27,57,71}

The limit of our spectral range in the NIR (7000–11 000 cm^{-1}) precludes the direct observation of transient absorption features that can be identified with the $2^1A_g^- \rightarrow 1^1B_u^+$ electronic origins ((0–0) bands). We thus considered several options for the assignments indicated in Figure 7. Our analysis of the room temperature and 77 K fluorescence spectra for $N =$

7 forces the assignment of the $2^1A_g^- \rightarrow 1^1B_u^+$ vibronic bands indicated in Figure 7. Comparison of the $2^1A_g^- \rightarrow 1^1B_u^+$ (0–2) and $1^1A_g^- \rightarrow 1^1B_u^+$ (0–2) energies for $N = 7$ then allows the direct calculation of the room temperature $2^1A_g^-$ zero-point energy as $18\,800 \pm 90 \text{ cm}^{-1}$ (532 nm). Figure 6 compares this estimate of the room temperature (0–0) band with the electronic origin observed in the 77 K $S_1 \rightarrow S_0$ fluorescence ($19\,900 \text{ cm}^{-1}$, 503 nm). The approximately 1000 cm^{-1} difference is consistent with the shift between the 77 K and room temperature emissions seen in Figures 5 and 6 and shifts noted in other polyenes (see above). The relatively broad $N = 7$ fluorescence spectrum at room temperature precludes the accurate measurement of the $S_1 \rightarrow S_0$ (0–0), but the shift in the vibronic envelope of the room temperature emission relative to the 77 K emission supports the assignments of the vibronic bands in the $2^1A_g^- \rightarrow 1^1B_u^+$ spectrum given in Figure 7. No other choice for these assignments can be reconciled with the $N = 7$ fluorescence spectra, and the central vibrational band that occurs $\sim 8500 \text{ cm}^{-1}$ for $N = 7$ –19 thus can be safely assigned to the (0–2) vibrational band of the $2^1A_g^- \rightarrow 1^1B_u^+$ transition. Comparisons between the (0–2) bands for the $2^1A_g^- \rightarrow 1^1B_u^+$ and $1^1A_g^- \rightarrow 1^1B_u^+$ transitions lead to the $2^1A_g^-$ energies presented in Table 2. As anticipated from Figure 7, the $1^1B_u^+ - 2^1A_g^-$ energy difference is essentially constant ($5900 \pm 200 \text{ cm}^{-1}$) for $N = 7$ –19 and also agrees well with our estimate ($5800 \pm 300 \text{ cm}^{-1}$) for the energy gap for $N = 5$, based on its room temperature absorption and emission spectra (see above). Measurements of the $1^1B_u^+ - 2^1A_g^-$ energy gap for a series of dimethyl polyenes indicated a small, systematic increase with conjugation length, i.e., the gap increases from $\sim 4500 \text{ cm}^{-1}$ for $N = 4$ to $\sim 6000 \text{ cm}^{-1}$ for $N = 7$ in room temperature hexane.⁵ Previous studies on natural and synthetic carotenoids with $N = 7$ –13 suggest that this gap approaches an asymptotic limit for large N , so the current results are consistent with the considerable amount of data on the excited state energies of short, model polyenes and carotenoids.^{27,45}

3.3. Electronic Energies of $1^1A_g^-$ and $1^1B_u^+$ States: Dependence of Transition Energies on Conjugation Length. **3.3.1. Assignments of Electronic Transitions.** The polyenes under study are constrained to planar, multi-*cis* structures by five-membered rings that include a *cis* double bond and have two polar R substituents, where $R = \text{CO}_2\text{CH}(\text{CH}_3)_2$ (Figure 1). When these groups were included in our calculations, we simplified R as $R' = \text{COOH}$. The structural and electronic influences of the polar R' groups and the five-membered rings were studied for the $N = 5$ polyenes using MNDO-PSDCI^{6,43} theory (Figure 8) and EOM-CCSD^{47–49} theory (Figure S2, Supporting Information). As

Table 2. State and Transition Energies (cm^{-1}) of Polyene Excited States in 2-MTHF^a

N	$1^1B_u^+$ ^b	$2^1A_g^-$ ^c	$2^1A_g^- \rightarrow 1^1B_u^+$ ^d	$2^1A_g^- \rightarrow n^1B_u^+$	$1^1B_u^+ \rightarrow n^1A_g^-$
7	24400	18800	5600	19700	11900
9	22100	16300	5800	17500	10600
11	20700	14700	6000	16000	9300
13	19800	13800	6000	14900	8500
15	19200	13100	6100	14100	8000
19	18400	12600	5800	~ 12800	< 7100

^aEstimated uncertainties ($\pm 1\sigma$) are $\sim 100 \text{ cm}^{-1}$ for the energies indicated. ^b(0–0) band from sum of Gaussian fits to the $1^1A_g^- \rightarrow 1^1B_u^+$ steady-state absorption. ^cCalculated from the difference between the (0–2) band of the $1^1A_g^- \rightarrow 1^1B_u^+$ steady-state absorption and the (0–2) band of the $2^1A_g^- \rightarrow 1^1B_u^+$ component from transient absorption. Peak positions were obtained from the sum of Gaussian fits. ^dDifference between $1^1B_u^+$ and $2^1A_g^-$ energies.

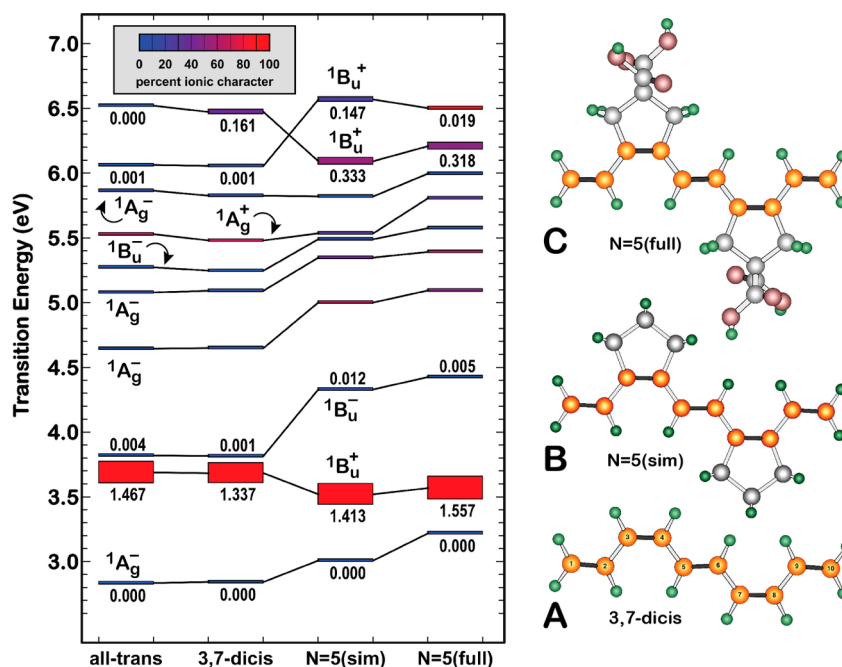


Figure 8. Impact of geometry and substituents on the calculated properties of the $N = 5$ polyene. The inset shows the calculated excited state level ordering based on MNDO-PSDCI calculations for the unsubstituted all-*trans* polyene, the unsubstituted 3,7-di-*cis* polyene (A), the 3,7-di-*cis* polyene with a simplified backbone (B), and the full $N = 5$ polyene including the ring substituents (C). Oscillator strengths for selected transitions and the relative ionic versus covalent character of each electronic state are indicated. Results for these four models based on EOM-CCSD methods are presented in Figure S2, Supporting Information.

shown in Figure 8, the backbone of rings has an important impact on the transition energies and oscillator strengths of all electronic transitions. However, the ordering of levels is not affected except in the higher energy regions. The R' group also has an effect, but in more subtle ways that likely would be masked by the polar solvent (2-MTHF) used to record the spectra. Because our primary interests in this study are the energies and intensities of polyene electronic transitions, we included the rings but excluded the R' groups in subsequent calculations.

We started our examination of the excited state level ordering by studying the absorption spectrum of the $N = 9$ polyene, which provides a viable target for both our semiempirical and *ab initio* methods. Comparisons of MNDO-PSDCI, SAC-CI, and EOM-CCSD calculations are presented in Figure S3, Supporting Information. Although the SAC-CI calculations were carried out at the highest standard level (LevelThree),^{50,53} a ${}^1B_u^+$ state is calculated to be the lowest-lying singlet state. This prediction is not consistent with the experimental results, which give strong evidence for a lowest-excited ${}^1A_g^-$ state. All the other methods predict $2{}^1A_g^-$ as the lowest excited singlet. Nevertheless, the SAC-CI calculations provide a good description of the electronic properties of the ionic ${}^1B_u^+$ states.

The EOM-CCSD calculations represent the highest-level of theory employed in this study and serve as the reference to which the other calculations should be compared. In most respects, the EOM-CCSD calculations are in excellent agreement with experiment. These methods predict a lowest excited $2{}^1A_g^-$ state and allowed ${}^1B_u^+$ states in all regions for which bands are observed in the room temperature absorption spectra. However, all transition energies are consistently underestimated by ~ 0.4 eV. Because the EOM-CCSD and MNDO-PSDCI calculations are in excellent agreement regarding transition energies and oscillator strengths, we used

the computationally faster MNDO-PSDCI methods to explore possible origins of the differences in the calculated versus observed transition energies. One possible source of error might be the assumption of planar C_{2h} (or C_{2v}) geometries. For example, these polyenes may be distorted slightly in polar solution around the single bonds to generate a corkscrew conformation, which creates a dipole moment along the polyene chain. This conformation previously was shown to be an important contributor to the absorption spectra of carotenoids.⁵⁷ A corkscrew conformation was generated for the $N = 9$ polyene by using B3LYP/6-31G(d) methods and solvent optimization utilizing the Polarizable Continuum Model (PCM)^{84–86} in acetonitrile. The resulting conformation exhibited small ($4\text{--}6^\circ$) dihedral distortions of the single bonds and generated a small blue shift in the transition energies (Figure S3, Supporting Information). Agreement with the experimental transition energies improved only slightly, and we concluded that the formation of corkscrew conformations is possible, but of minimal importance in understanding the spectra of these conformationally constrained molecules.

All the theoretical treatments are in agreement that the only electronic transitions with detectable oscillator strength originating in the ground state are ${}^1A_g^- \rightarrow {}^1B_u^+$ (Figure 9). It may surprise the observer that transitions to ${}^1A_g^+$ states, which are responsible for the distinctive *cis*-bands in polyene and carotenoid electronic spectra,^{30,87,88} do not have detectable intensities in these systems. However, the *cis* linkages in these molecules are symmetrically placed and do not generate mixing between the gerade and ungerade excited states to yield oscillator strength in the ${}^1A_g^- \rightarrow {}^1A_g^+$ transitions. The inherent simplicity of the absorption spectra of these polyenes thus is associated, in large part, with the lack of participation of ${}^1A_g^+$ states in absorption.

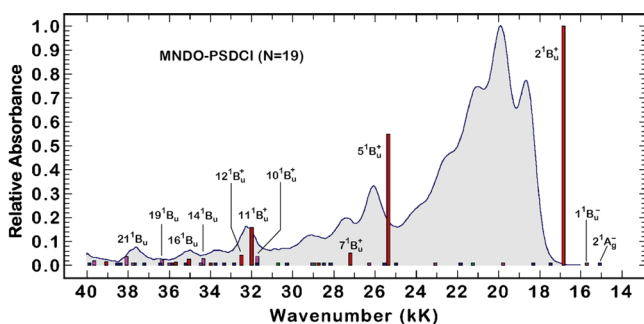


Figure 9. Electronic transitions predicted by MNDO-PSDCI molecular orbital theory are superimposed on the absorption spectrum of the $N = 19$ polyene ($1 \text{ kK} = 10^3 \text{ cm}^{-1}$). The heights of the vertical bars are proportional to the calculated oscillator strengths of the transitions. The calculations included the simplified backbone system (Figure 8B) and included full single and double configuration interaction within the π -system. Note that all of the allowed states are ${}^1\text{B}_u^+$ states. The ionic (+) versus covalent (-) character of these states is mixed at higher energies to such an extent that assignment of ionic versus covalent character is not possible.

The MNDO-PSDCI calculations on $N = 19$ (Figure 9) also indicate the possible presence of a second dark state (${}^1\text{B}_u^-$) below the ${}^1\text{B}_u^+$ state responsible for the major absorption in these molecules. A low-energy ${}^1\text{B}_u^-$ state was predicted in early calculations on longer polyenes by Tavan and Schulten⁸⁹ and in more recent theoretical studies.^{30,90–92} Although Raman excitation studies^{91,92} and two-photon polarization studies⁶ have reported evidence for this state, the ${}^1\text{B}_u^-$ state has not been observed in direct UV–visible absorption experiments, nor is there any compelling evidence for the ${}^1\text{B}_u^-$ state in the excited state dynamics of these polyenes or corresponding carotenoids.

3.3.2. Dependence of Electronic Energies on Conjugation Length: Implications for the Excited State Energies of Infinite Polyenes. The lowest energy electronic transitions in the visible and NIR transient absorption experiments for $N = 7–19$ are summarized in Table 2 and in Figure 10. On the basis of these transition energies and the energies of the ${}^1\text{A}_g^- \rightarrow {}^1\text{B}_u^+$ transition, the energies of additional excited electronic states can be calculated and compared with the allowed electronic states seen directly in absorption, e.g., ${}^1\text{A}_g^- \rightarrow {}^1\text{B}_u^+$. The current studies, combined with the transition energies observed in the unusually well-resolved steady-state absorption spectra (Figure 2 and Scriban et al.³²), provide an unusually rich set of data (Table S2, Supporting Information) on the low-lying singlet states (${}^1\text{A}_g^-$ and ${}^1\text{B}_u^+$) of this homologous series of polyenes over a wide range of conjugation lengths ($N = 5–23$). The data summarized in Figure 11 (and Tables 2 and S2, Supporting Information) offer some straightforward challenges for improving theoretical descriptions of polyene excited states, including understanding the electronic structures in the infinite polyene limit.

The assignments of the absorption spectra are supported by MNDO-PSDCI, SAC-CI, and EOM-CCSD calculations on $N = 5$ and $N = 9$ (Figure 8, S2, and S3, Supporting Information) and on the MNDO-PSDCI calculations on $N = 19$ (Figure 9). All the transitions in the steady-state, room temperature absorption spectra, including the strongly allowed transition that dominates all polyene spectra, are assigned to ${}^1\text{A}_g^- \rightarrow {}^1\text{B}_u^+$ transitions. As discussed above, the weak ${}^1\text{A}_g^- \rightarrow {}^1\text{A}_g^-$ transitions (*cis* bands) observed in the absorption spectra of

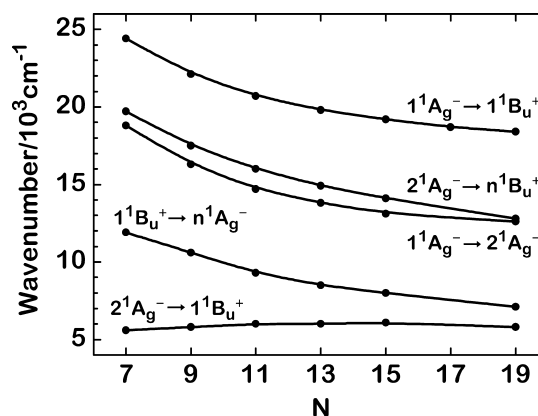


Figure 10. Polyene transition energies in room temperature 2-MTHF. Data from Table 2. Energies of the ${}^1\text{A}_g^- \rightarrow {}^1\text{B}_u^+$ transition (0–0) were obtained from the sum of Gaussian fits. Energies of the ${}^2\text{A}_g^- \rightarrow n^1\text{B}_u^+$ and ${}^1\text{B}_u^+ \rightarrow n^1\text{A}_g^-$ transitions correspond to the wavelengths of maximum absorption of EADS components from the transient absorption spectra. The ${}^1\text{A}_g^- \rightarrow {}^2\text{A}_g^-$ transition energy was calculated from the difference between the (0–2) band of the ${}^1\text{A}_g^- \rightarrow {}^1\text{B}_u^+$ steady-state absorption and the (0–2) band of the ${}^2\text{A}_g^- \rightarrow {}^1\text{B}_u^+$ transient absorption. Peak positions were obtained from the sum of Gaussian fits.

carotenoids and *cis*-polyenes do not have detectable oscillator strengths in these symmetric, alternating, *cis*–*trans* polyene systems. The oscillator strengths of the symmetry-allowed transitions to ${}^1\text{B}_u^+$ states systematically decrease for transitions into higher energy states, and this pattern is supported by the calculations. The transient absorption spectra also involve symmetry-allowed transitions: ${}^2\text{A}_g^- \rightarrow {}^1\text{B}_u^+$, ${}^2\text{A}_g^- \rightarrow n^1\text{B}_u^+$, and ${}^1\text{B}_u^+ \rightarrow n^1\text{A}_g^-$. In combination with the ${}^1\text{A}_g^- \rightarrow {}^1\text{B}_u^+$ transition energies, the transient absorption spectra thus allow calculations of the energies of ${}^2\text{A}_g^-$, $n^1\text{A}_g^-$, and the state labeled as $n^1\text{B}_u^+$. The electronic energies obtained by combining the steady-state absorption data of Scriban et al.³² and the data from the transient absorption experiments are summarized in Figure 11 and Tables 2 and S2, Supporting Information.

The data presented in Figure 11 show remarkably simple patterns, which allow extrapolation of energies to large N . All of the ${}^1\text{B}_u^+$ states, including the ${}^1\text{B}_u^+$ state detected in the transient absorption spectra exhibit a systematic nonlinear dependence with respect to $1/N$. Deviations from a linear dependence, previously assumed for the electronic energies of shorter polyenes and carotenoids, are most obvious in this series, due to the large range of N values and the number of electronic states we have been able to detect and assign. The curvature in the data (Figure 11) can be accounted for by including an additional term in the least-squares fits. Separate quadratic fits to each of the ${}^1\text{B}_u^+$ states suggested a common asymptotic limit of $15\,000 \pm 1\,000 \text{ cm}^{-1}$. We thus did a global fit to all of the ${}^1\text{B}_u^+$ energies, assuming a common, unspecified value at $1/N = 0$. This global fit established an extrapolated ${}^1\text{B}_u^+$ energy of $15\,870 \pm 94 \text{ cm}^{-1}$. Including this value in individual fits to each ${}^1\text{B}_u^+$ state resulted in the quadratic fits indicated in Figure 11 and summarized in Table S3, Supporting Information. This asymptotic limit is remarkably consistent with the vibronically resolved 77 K absorption spectrum of a related polyene polymer ($1/N \approx 0$), containing a mixture of five- and six-membered rings, which shows a single, prominent absorption (${}^1\text{A}_g^- \rightarrow {}^1\text{B}_u^+$) with an electronic origin at $15\,800 \text{ cm}^{-1}$.⁹³ As

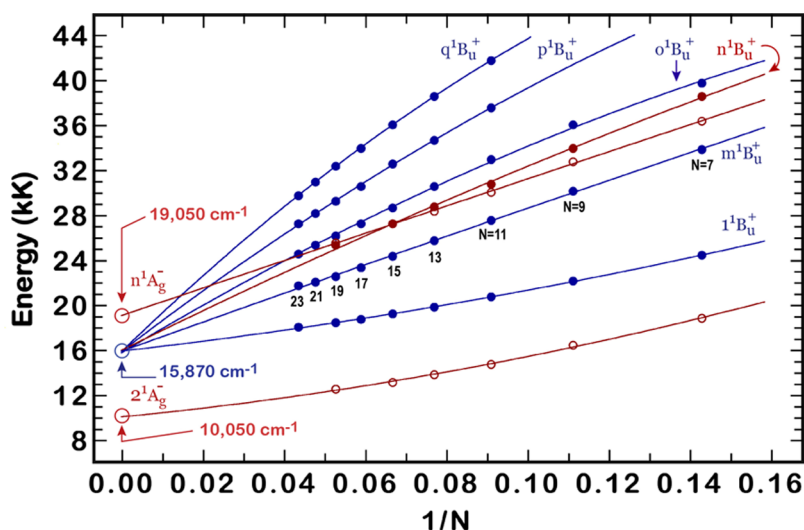


Figure 11. Electronic transition energies of $N = 7\text{--}23$ polyenes in room temperature 2-MTHF (data from Table S2, Supporting Information) ($1 \text{ kK} = 10^3 \text{ cm}^{-1}$). Data points and lines in blue correspond to absorption measurements, and data points and lines in red are derived from transient absorption measurements. Open circles designate measurements of ${}^1A_g^-$ state energies, and solid circles designate measurement of ${}^1B_u^+$ states energies. Lines are from quadratic fits ($E = A + B/N + C/N^2$) as explained in the text. Parameters of the fits are presented in Table S3, Supporting Information.

discussed previously,⁹³ the convergence of all of the allowed transition energies in the infinite polyene limit accounts for the very simple, well-resolved absorption spectrum of the unpurified polymer. It is important to note that this convergence was predicted by the early multireference double-excitation configuration interaction (MRDCI) calculations of Tavan and Schulten,⁸⁹ which indicate a common energy for all ionic states (${}^1B_u^+$ and ${}^1A_g^+$) for $N = \infty$. The current studies cannot detect any ${}^1A_g^+$ states, due to the vanishingly small ${}^1A_g^- \rightarrow n^1A_g^+$ transition dipoles (*cis* bands) in these polyene systems.

Tavan and Schulten⁸⁹ also predicted a similar convergence of the excited covalent states (${}^1A_g^-$ and ${}^1B_u^-$), but a common asymptotic limit clearly is not supported by the data for the $2^1A_g^-$ and $n^1A_g^-$ states shown in Figure 11. The two ${}^1A_g^-$ states are separated by $\sim 9000 \text{ cm}^{-1}$ in the infinite polyene. We explored both theoretically and experimentally the possibility that the difference in the transition energies of the two ${}^1A_g^-$ states could be due to the different spectroscopic methods used to assign the state energies. Note that the higher energy $n^1A_g^-$ state was observed via transient absorption spectroscopy from the first excited ${}^1B_u^+$ state. We examined the possibility that an evolved ${}^1B_u^+$ state would decrease in energy relative to the higher $n^1A_g^-$ state to yield a blue-shifted transition energy. Although EOM-CCSD and MNDO-PSDCI calculations predict that an evolved ${}^1B_u^+$ state indeed shifts to lower energy, the calculations indicate that the higher ${}^1A_g^-$ state, which is optically coupled to the ${}^1B_u^+$ state, drops by a comparable amount. In our simulations, the largest ${}^1B_u^+ \rightarrow {}^1A_g^-$ shift induced by excited state evolution was a 300 cm^{-1} blue shift calculated for $N = 5$ (Figure S4, Supporting Information), which is negligible compared to the observed separation of $\sim 9000 \text{ cm}^{-1}$. Furthermore, the relative shifts of these states decrease as the conjugation length increases. Our calculations show that the rigid structures of these polyenes is partially responsible for preventing excited state evolution from creating significant shifts in the measured absolute state energies.

The theoretical analysis is supported by the time independence of the ${}^1B_u^+ \rightarrow n^1A_g^-$ transient absorption

profiles during the 100–200 fs lifetime of the ${}^1B_u^+$ state (Figure 4). Additional experimental support for the viability of the $\sim 9000 \text{ cm}^{-1}$ separation between the ${}^1A_g^-$ states is that one of the six ${}^1B_u^+$ states included in the extrapolations ($n^1B_u^+$) also was observed via transient absorption. This state, designated by closed red circles and a red line in Figure 11, extrapolates to the same infinite polyene limit as for the ${}^1B_u^+$ states detected in the steady-state absorption spectra. We conclude with confidence that the two ${}^1A_g^-$ states assigned in this study extrapolate to significantly different infinite polyene limits and that the 9000 cm^{-1} separation is intrinsic to the energies of the manifold of ${}^1A_g^-$ states rather than an experimental artifact.

3.4. Energy Gap Law Analysis of $2^1A_g^-$ Lifetimes.

3.4.1. Comparisons with Carotenoids. The lifetimes (τ_1) of the $2^1A_g^-$ states of these polyenes are dominated by nonradiative decay to the ground state and show a significant decrease with conjugation length, ranging from 370 ps for $N = 7$ to 0.50 ps for $N = 19$ (Table 1). The energy gap law⁶⁶ predicts that the rate of nonradiative decay depends approximately exponentially on the $2^1A_g^- - 1^1A_g^-$ energy difference, which in turn depends approximately inversely on the conjugation length (Figure 11). A simple application of the energy gap law for the current series is presented in Figure 12 and compared with a similar analysis of $2^1A_g^-$ lifetimes and energies for several open-chain, all-*trans* carotenoids (Table S4, Supporting Information). Both sets of molecules exhibit linear relationships between the log of the $2^1A_g^-$ decay constant and the $2^1A_g^-$ energy determined from transient absorption experiments. Although additional data on $2^1A_g^-$ energies and lifetimes is available from fluorescence measurements, previous work²⁹ has shown that the fluorescence of longer ($N > 7$), all-*trans* polyenes is dominated by emission from less symmetric *cis* impurities or by distorted *trans* isomers, either present in the ground state or formed in the $2^1A_g^-$ state following the excitation of more symmetric, all-*trans* species. Steady-state and time-resolved fluorescence experiments of longer polyenes thus may favor the detection of nonrepresentative subsets of $2^1A_g^-$ conformers and geometric isomers, even for highly purified samples with relatively narrow distributions of all-*trans* ground

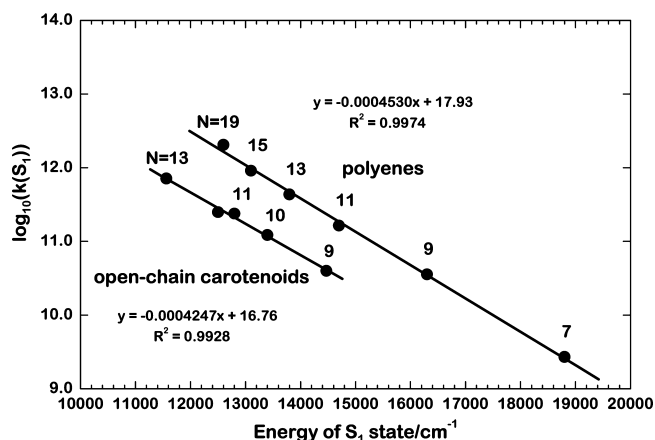


Figure 12. Simplified energy gap law analysis of $2^1A_g^-$ lifetimes for constrained polyenes and open-chain carotenoids. k is $1/\tau_1$ from Tables 1 and S4, Supporting Information. Parameters for the linear fits are indicated.

state conformers. Measurements of the $2^1A_g^-$ energies and lifetimes by detection of the symmetry allowed $2^1A_g^- \rightarrow 1^1B_u^+$ and $2^1A_g^- \rightarrow n^1B_u^+$ transitions thus provide a more reliable set of data for exploring the connections between $2^1A_g^-$ decay rates and energies.

Figure 12 shows excellent fits to the energy gap law for the open-chain carotenoids ($N = 9-13$) and the polyenes ($N = 7-19$). This figure illustrates the uniformly lower $2^1A_g^-$ energies ($\sim 2000 \text{ cm}^{-1}$) for carotenoids with a given N . The nonradiative decay rates also are systematically smaller for the carotenoids, and these counteracting effects result in $2^1A_g^-$ lifetimes that are quite comparable for polyenes and open-chain carotenoids with the same conjugation length, cf. $\tau_1 = 4.5 \text{ ps}$ for lycopene vs $\tau_1 = 6.1 \text{ ps}$ for the $N = 11$ polyene. Comparison between these two series (Figure 13) illustrates the very similar nonradiative decay

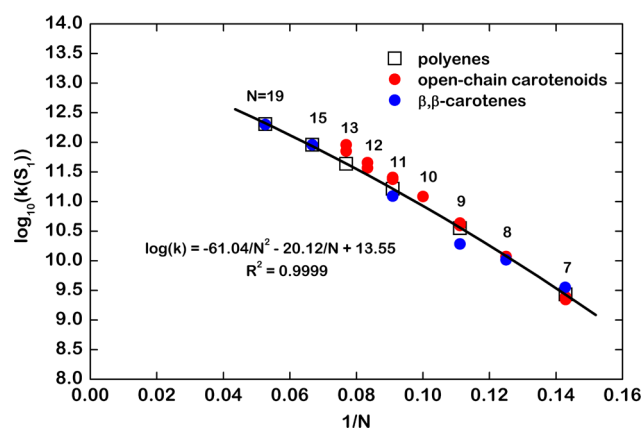


Figure 13. $\log_{10}(k(S_1))$ versus $1/N$ for constrained polyenes, open-chain carotenoids, and β,β -carotenes. k is $1/\tau_1$ from Tables 1 and S4, Supporting Information. Red data points are open-chain carotenoids with $N = 7-13$; blue data points are β,β -carotenes with $N = 7-19$. Quadratic fit is to data for constrained polyenes.

rates for molecules with a given N . Longer open-chain carotenoids tend to have slightly shorter lifetimes than their polyene counterparts, but the $2^1A_g^-$ dynamics are rather similar. To underscore this point, we also include data for β -carotene and its synthetic analogues ($N = 9-19$). Note (Table S4, Supporting Information) that the $2^1A_g^-$ lifetimes for the $N = 15$

and $N = 19$ analogues of β -carotene are identical to the $2^1A_g^-$ lifetimes measured for the polyene series, i.e., 1.1 and 0.5 ps.²⁵ The data for the three series (Figure 13 and Table S4, Supporting Information) reinforce the conclusion that the length of conjugation is the primary determinant of $2^1A_g^-$ dynamics for a wide range of polyenes and carotenoids. The decay rates with the largest deviations from this simple pattern (corresponding to β -carotene analogues with $N = 7, 8$, and 9) are those whose lifetimes were determined using fluorescence techniques, rather than by transient absorption. This further emphasizes that the weak, symmetry-forbidden fluorescent signals detected in these systems likely are not representative of the all-*trans* conformers that dominate the distributions of ground state geometries.

We explored the possibility that the $2^1A_g^-$ state converts to the ground state via population of a conical intersection. Theoretical studies suggest that such features are present in many polyenes,⁹⁴⁻⁹⁶ and we investigated this for the $N = 5$ and $N = 7$ polyenes using CASSCF methods as implemented in Gaussian09. Our tentative conclusion is that the rigid backbone of rings (Figure 1) provides structural constraints that prevent the adiabatic formation of conical intersections, but the observation of nearly degenerate avoided crossings indicates that such features may be present in the larger polyenes. The relatively long lifetimes of the $2^1A_g^-$ states in the $N = 5$ and 7 polyenes (Table 1) suggest that, while conical intersections might well be part of the excited state landscape, the population of these features is not kinetically favorable. The much shorter lifetimes of the $2^1A_g^-$ states in the longer polyenes implies that conical intersections may play roles in $2^1A_g^- \rightarrow 1^1A_g^-$ internal conversions for polyenes with $N > 7$. However a more detailed analysis of the potential of conical intersections to account for the data summarized in Figures 12 and 13 is beyond the purview of this article.

3.4.2. Excited State Dynamics of Infinite Polyenes. The data summarized in Figures 11-13 also allow us to speculate on the excited state dynamics of infinite polyenes. As discussed in the previous section, extrapolation of the energies of the symmetry allowed transitions ($\sim 15900 \text{ cm}^{-1}$ in the infinite polyene limit) is in good agreement with the (0-0) energy for the $1^1A_g^- \rightarrow 1^1B_u^+$ transition in a related polymer (DEDPM) with $1/N \approx 0$.⁹³ Extrapolation of the $2^1A_g^-$ energies gives a limiting energy at $\sim 10000 \text{ cm}^{-1}$, consistent with the constant, $\sim 5900 \text{ cm}^{-1}$ $1^1B_u^+ - 2^1A_g^-$ energy gap noted in Figure 7 and Table 2.

The $2^1A_g^-$ lifetime data (τ_1) for $N = 7-19$ (Figure 13) extrapolates to a $2^1A_g^-$ lifetime of $\sim 30-40 \text{ fs}$ for the infinite polyene. However, we expect limits to the time scales in which these molecules convert electronic energy into vibrational energy, which raises the question whether a $< 100 \text{ fs}$ $2^1A_g^-$ lifetime can be realized. The convergence of the $2^1A_g^-$ and $1^1B_u^+$ lifetimes (τ_1 and τ_2 , Table 1) for polyenes with large N complicates the analysis of the excited state kinetics and the transient absorption spectra. Nevertheless, comparison of the data presented here for the $N = 7-19$ polyenes with recent femtosecond pump-probe experiments on the DEDPM polymer in room temperature THF narrows the range of the $2^1A_g^-$ lifetime in the limit of infinite N .⁹⁷ The molar mass and polydispersity of the DEDPM sample translates into polymers with 3300 ± 760 double bonds. Synthetic defects in the polymerization reactions, chemical and photochemical degradation, and conformational disorder, especially in room temperature solutions, most likely result in distributions of

considerably shorter conjugated segments, but the absorption spectra appear to be dominated by molecules with conjugation lengths >50 .⁹³ The transient absorption spectra of DEDPM thus should be representative of species with $1/N \approx 0$, especially for samples excited on the red edge of the broad absorption band. Antognazza et al.⁹⁷ in ultrafast pump–probe experiments (10 fs time resolution) on room temperature THF solutions of DEDPM isolated decay components of 17, 50, 175, and 1200 fs. The first two components were assigned to the depopulation of the $1^1B_u^+$ state (17 fs) to a hot $2^1A_g^-$ state via an intermediate state denoted S_x (50 fs). Vibrational relaxation of the $2^1A_g^-$ state was associated with the 175 fs component, and the 1200 fs component was assigned to radiationless decay from the zero-point level of $2^1A_g^-$ into the ground state. Our analysis of the kinetic components of polyenes with $N = 7–19$ (Table 1), however, makes it unlikely that a polyene with $1/N \approx 0$ could have a $2^1A_g^-$ lifetime longer than 1 ps. Thus, the 1200 fs feature observed by Antognazza et al.⁹⁷ most likely is due to the decay of the S^* signal, a hypothesis that also is supported by the shape of the species-associated spectrum of this component. The 500 fs $2^1A_g^-$ lifetime of the $N = 19$ polyene then makes it plausible to assign the 175 fs component in DEDPM to the decay of the relaxed $2^1A_g^-$ state, which is considerably longer than the 30–40 fs lifetime predicted by the linear extrapolation presented in Figure 13.

4. CONCLUSIONS

(1) We have carried out detailed experimental and theoretical studies on the low-lying electronic states of a series of synthetic, constrained polyenes with 5–23 conjugated double bonds (N). The rigid geometries of these molecules result in vibronically resolved electronic spectra, even in room temperature solutions.³² This has allowed a systematic investigation of the energies of several allowed ($1^1B_u^+$) and forbidden ($1^1A_g^-$) electronic states as a function of conjugation length.

(2) We have recorded steady-state UV and visible absorption spectra for $N = 5–23$ and ultrafast transient absorption spectra for $N = 7–19$ in the visible and NIR spectral regions. Absorption and fluorescence spectra of the $N = 5$ and $N = 7$ polyenes, both in room temperature solutions and in 77 K glasses, proved critical in assigning the vibronic bands of the symmetry-allowed, $2^1A_g^- \rightarrow 1^1B_u^+$ transitions detected in the NIR transient absorption experiments. The energies of the $2^1A_g^- \rightarrow 1^1B_u^+$ transitions from the time-resolved absorption measurements were subtracted from the energies of the strongly allowed $1^1A_g^- \rightarrow 1^1B_u^+$ transitions obtained from steady-state absorption spectra to yield the $2^1A_g^-$ energies for $N = 7–19$ (Table 2). We find that the $1^1B_u^+ - 1^1A_g^-$ energy gap of $5900 \pm 200 \text{ cm}^{-1}$ is invariant to polyene length for $N = 7–19$ in room temperature 2-MTHF.

(3) EOM-CCSD ab initio and MNDO-PSDCI semiempirical MO calculations facilitated the assignments of six $1^1B_u^+$ states and two excited $1^1A_g^-$ states in the steady-state and transient absorption spectra. Both theories account for the experimental transition energies and intensities, provided the aliphatic rings are included in the calculations and predict that only the $1^1A_g^- \rightarrow 1^1B_u^+$ transitions have sufficient oscillator strength to be observed in the steady-state absorption spectra. Analysis of the N dependence of the $1^1B_u^+$ energies indicates that the six ionic states extrapolate to an infinite polyene energy of $\sim 15\,900 \text{ cm}^{-1}$ (Figure 11). This energy is in excellent agreement with the electronic origin of the $1^1A_g^- \rightarrow 1^1B_u^+$ transition of a related conjugated polymer (DEDPM) with very large N .⁹³ The

convergence of the $1^1B_u^+$ states to a common, infinite polyene limit agrees with the early theoretical predictions of Tavan and Schulten.⁸⁹ The two excited $1^1A_g^-$ states exhibit a substantial ($\sim 9000 \text{ cm}^{-1}$) energy difference in the infinite polyene limit (Figure 11), in contrast to the common limit for covalent states ($1^1A_g^-$ and $1^1B_u^-$) predicted by previous theoretical treatments.⁸⁹ The EOM-CCSD calculations indicate that this energy difference cannot be associated with the time-evolution of the relevant excited states.

(4) The ultrafast transient absorption experiments provide detailed information on the dynamics of the excited states following photoexcitation into the $1^1B_u^+$ state. The kinetic data confirm the assignments of transitions originating from both the $2^1A_g^-$ and the $1^1B_u^+$ states and provide insights on the decay pathways of these states. The transient absorption spectra, EADS components, and excited state lifetimes of these constrained polyenes are remarkably similar to those of less rigid, less symmetric, biologically relevant carotenoids with comparable conjugation lengths.^{45,57,71} These similarities include the longer-lived S^* components observed in polyenes with $N = 13, 15,$ and 19 . Comparisons with previous ultrafast studies of the dynamics of the low-lying excited states of carotenoids are important for elucidating the mechanisms by which naturally occurring polyenes carry out their light-harvesting and photoprotective roles in biological systems.

(5) The $2^1A_g^-$ lifetimes are well-accounted for by the $2^1A_g^- - 1^1A_g^-$ energy differences, following the energy gap law for radiationless decay. As shown in Figure 13, the decay kinetics of these rigid polyenes as a function of N are in remarkable agreement with N dependence of the $2^1A_g^-$ decay rates of both open-chain carotenoids and analogues of β -carotene. For example, for the $N = 11$ polyene, lycopene ($N = 11$), and β -carotene ($N = 11$), the $2^1A_g^-$ lifetimes are 6.1, 4.0, and 8.1 ps, respectively.^{98,99}

(6) The excited state dynamics for the $N = 7–19$ polyenes also have allowed us to revisit previous ultrafast experiments on the infinite polyene, the related DEDPM polymer.⁹⁷ Extrapolation of the $2^1A_g^-$ lifetimes for the polyene series suggests a 30–40 fs lifetime in the infinite polyene limit. However, our analysis of the DEDPM kinetic data⁹⁷ points to a 175 fs $2^1A_g^-$ lifetime and a 1200 fs component that we assign to the decay of the S^* state.

(7) Transient signals assigned to S^* states in previous studies of long carotenoids are observed for the $N = 13, 15,$ and 19 polyenes. Similar signals in the long carotenoids have been ascribed to conformational twisting within $2^1A_g^-$.^{45,57,67} However, the restricted range of torsional motions available to these highly constrained polyenes on their $2^1A_g^-$ potential surfaces significantly limits the rearrangements required to account for the prominent S^* signals in both sets of molecules. For the $N = 19$ polyene, the rise of S^* parallels the decay of the $2^1A_g^-$ state, suggesting that these S^* signals may be due to $1^1A_g^- \rightarrow 1^1B_u^+$ absorption from excited vibrational levels of the ground state ($1^1A_g^-$), as originally proposed by Gillbro et al.²⁵ However, this model cannot explain the dynamics of the $N = 13$ and 15 polyenes or the S^* signals in spirilloxanthin ($N = 13$) or rhodoxanthin ($N = 14$).^{76–78} For all of these molecules, the S^* signals appear well in advance of the >1 ps decay times of the $2^1A_g^-$ states. Understanding which of the two models for the S^* signals is appropriate under what conditions will require more extensive experimental and theoretical efforts on this polyene series. Further studies should result in the development of a more comprehensive kinetic model for the excited state

decays of both synthetic and naturally occurring polyenes as a function of their conjugation lengths, structural features, and solvent environments.

■ ASSOCIATED CONTENT

● Supporting Information

Table S1 gives the group correlation table and selection rules for $\pi\pi^*$ electronic transitions for molecules with C_{2h} and C_{2v} symmetries and closed-shell electronic ground states. Table S2 gives the electronic transition energies of the $N = 7-23$ polyenes shown in Figure 11. Table S3 gives the individual quadratic fits to the electronic transition energies given in Table S2. Table S4 compares the energies and lifetimes in room temperature solvents of the S_1 ($2^1A_g^-$) excited states of constrained polyenes, all-*trans* open-chain carotenoids, and all-*trans* β,β -carotenoids. Figure S1 gives kinetic traces associated with the $2^1A_g^- \rightarrow n^1B_u^+$ and $S^* \rightarrow n^1B_u^+$ transient absorptions for $N = 19$. Least squares fits and associated rise and decay times of these signals are indicated. The impacts of geometry and substituents on the calculated energies and oscillator strengths of the $N = 5$ polyene are shown in Figure S2. The EOM-CCSD calculations compare the excited states for the unsubstituted all-*trans* polyene, the unsubstituted 3,7-di-*cis* polyene, the 3,7-di-*cis* polyene with a simplified backbone, and the full $N = 5$ polyene with the ring substituents. Calculations on $N = 9$ with a simplified backbone are superimposed on the observed absorption spectrum in Figure S3. This figure compares spectra predicted by SAC-CI, EOM-CCSD, and MNDO-PSDCI calculations, and a MNDO-PSDCI calculation on a corkscrew, non- C_{2h} conformation, which was optimized in room temperature acetonitrile. Figure S4 presents EOM-CCSD calculations on the $N = 5$ polyene for various conformations and relaxations. The key observation is that relaxation in the excited singlet state manifold alters the $1^1B_u^+ \rightarrow n^1A_g^-$ transition energy by less than 300 cm^{-1} . This material is available free of charge via the Internet at <http://pubs.acs.org>.

■ AUTHOR INFORMATION

Corresponding Author

*E-mail: rchrste@bowdoin.edu (R.L.C.); harry.frank@uconn.edu (H.A.F.); rberge@uconn.edu (R.R.B.). Phone: 207-725-3604 (R.L.C.); 860-486-2844 (H.A.F.); 860-486-6721 (R.R.B.). Fax: 207-725-3017 (R.L.C.); 860-486-2981 (R.R.B. and H.A.F.).

Author Contributions

[#]These authors contributed equally to this work.

Notes

The authors declare no competing financial interest.

■ ACKNOWLEDGMENTS

We wish to thank Katharina Bilotti for preliminary work on the purification and spectroscopy of these samples and Dr. Marcel Fuciman and Prof. George Gibson for technical assistance with the ultrafast laser system. R.L.C. was supported by the Petroleum Research Fund, administered by the American Chemical Society. R.R.S. acknowledges the Department of Energy (DE-FG02-86ER13564) for research support. T.P. thanks the Czech Ministry of Education for financial support (Grant No. ME09037). Work in the laboratory of H.A.F. was supported by grants from the National Science Foundation (MCB-0913022) and the University of Connecticut Research Foundation. Work in the laboratory of R.R.B. was supported by

grants from the National Science Foundation (EMT-0829916), the National Institutes of Health (GM-34548), and the Harold S. Schwenk Sr. Distinguished Chair in Chemistry.

■ REFERENCES

- (1) Hudson, B. S.; Kohler, B. E. *Chem. Phys. Lett.* **1972**, *14*, 299–304.
- (2) Hudson, B. S.; Kohler, B. E. *Annu. Rev. Phys. Chem.* **1974**, *25*, 437–460.
- (3) Hudson, B. S.; Kohler, B. E.; Schulten, K. In *Excited States*; Lim, E. D., Ed.; Academic Press: New York, 1982; Vol. 6, pp 1–95.
- (4) Pierce, B.; Bennett, J.; Birge, R. J. *Chem. Phys.* **1982**, *77*, 6343–6344.
- (5) Christensen, R. L.; Galinato, M. G. I.; Chu, E. F.; Howard, J. N.; Broene, R. D.; Frank, H. A. *J. Phys. Chem. A* **2008**, *112*, 12629–12636.
- (6) Shima, S.; Ilagan, R. P.; Gillespie, N.; Sommer, B. J.; Hiller, R. G.; Sharples, F. P.; Frank, H. A.; Birge, R. R. *J. Phys. Chem. A* **2003**, *107*, 8052–8066.
- (7) Frank, H. A.; Christensen, R. L. In *Carotenoids*; Britton, G., Liaaen-Jensen, S., Pfander, H., Eds.; Birkhäuser: Basel, Switzerland, 2008; Vol. 4, pp 167–188.
- (8) Schulten, K.; Karplus, M. *Chem. Phys. Lett.* **1972**, *14*, 305–309.
- (9) Schulten, K.; Ohmine, I.; Karplus, M. *J. Chem. Phys.* **1976**, *64*, 4422–4441.
- (10) Christensen, R. L. In *The Photochemistry of Carotenoids*; Frank, H. A., Young, A. J., Britton, G., Cogdell, R. J., Eds.; Kluwer Academic Publishers: Dordrecht, The Netherlands, 1999; Vol. 8, pp 137–159.
- (11) D'Amico, K. L.; Manos, C.; Christensen, R. L. *J. Am. Chem. Soc.* **1980**, *102*, 1777–1782.
- (12) Christensen, R. L.; Kohler, B. E. *J. Phys. Chem.* **1976**, *80*, 2197–2200.
- (13) Auerbach, R. A.; Christensen, R. L.; Granville, M. F.; Kohler, B. E. *J. Chem. Phys.* **1981**, *74*, 4–9.
- (14) Christensen, R. L.; Kohler, B. E. *J. Chem. Phys.* **1975**, *63*, 1837–1846.
- (15) Granville, M. F.; Holtom, G. R.; Kohler, B. E.; Christensen, R. L.; D'Amico, K. L. *J. Chem. Phys.* **1979**, *70*, 593–597.
- (16) Granville, M. F.; Holtom, G. R.; Kohler, B. E. *J. Chem. Phys.* **1980**, *72*, 4671–4675.
- (17) Petek, H.; Bell, A. J.; Yoshihara, K.; Christensen, R. L. *J. Chem. Phys.* **1991**, *95*, 4739–4750.
- (18) Petek, H.; Bell, A. J.; Choi, Y. S.; Yoshihara, K.; Tounge, B. A.; Christensen, R. L. *J. Chem. Phys.* **1993**, *98*, 3777–3794.
- (19) Petek, H.; Bell, A. J.; Choi, Y. S.; Yoshihara, K.; Tounge, B. A.; Christensen, R. L. *J. Chem. Phys.* **1995**, *102*, 4726–4739.
- (20) Buma, W. J.; Kohler, B. E.; Shaler, T. A. *J. Chem. Phys.* **1992**, *96*, 399–407.
- (21) Birge, R. R.; Bennett, J. A.; Pierce, B. M.; Thomas, T. M. *J. Am. Chem. Soc.* **1978**, *100*, 1533–1539.
- (22) Birge, R.; Bennett, J.; Hubbard, L.; Fang, H.; Pierce, B.; Klinger, D.; Leroi, G. *J. Am. Chem. Soc.* **1982**, *104*, 2519–2525.
- (23) Frank, H. A.; Cogdell, R. J. In *Carotenoids in Photosynthesis*; Young, A., Britton, G., Eds.; Springer-Verlag: London, 1993; pp 252–326.
- (24) Bondarev, S. L.; Knyuksho, V. N. *Chem. Phys. Lett.* **1994**, *225*, 346–350.
- (25) Andersson, P. O.; Gillbro, T. *J. Chem. Phys.* **1995**, *103*, 2509–2519.
- (26) Cosgrove, S. A.; Guite, M. A.; Burnell, T. B.; Christensen, R. L. *J. Phys. Chem.* **1990**, *94*, 8118–8124.
- (27) Polívka, T.; Herek, J. L.; Zigmantas, D.; Akerlund, H. E.; Sundström, V. *Proc. Natl. Acad. Sci. U.S.A.* **1999**, *96*, 4914–4917.
- (28) Polívka, T.; Zigmantas, D.; Frank, H. A.; Bautista, J. A.; Herek, J. L.; Koyama, Y.; Fujii, R.; Sundström, V. *J. Phys. Chem. B* **2001**, *105*, 1072–1080.
- (29) Christensen, R. L.; Galinato, M. G. I.; Chu, E. F.; Fujii, R.; Hashimoto, H.; Frank, H. A. *J. Am. Chem. Soc.* **2007**, *129*, 1769–1775.

- (30) Pendon, Z. D.; Sullivan, J. O.; van der Hoef, I.; Lugtenburg, J.; Cua, A.; Bocian, D. F.; Birge, R. R.; Frank, H. A. *Photosynth. Res.* **2005**, *86*, 5–24.
- (31) Czekelius, C.; Hafer, J.; Tonzetich, Z. J.; Schrock, R. R.; Christensen, R. L.; Müller, P. *J. Am. Chem. Soc.* **2006**, *128*, 16664–16675.
- (32) Scriban, C.; Amagai, B. S.; Stemmler, E. A.; Christensen, R. L.; Schrock, R. R. *J. Am. Chem. Soc.* **2009**, *131*, 13441–13452.
- (33) DeCoster, B.; Christensen, R. L.; Gebhard, R.; Lugtenburg, J.; Farhoosh, R.; Frank, H. A. *Biochim. Biophys. Acta* **1992**, *1102*, 107–114.
- (34) Christensen, R. L.; Kohler, B. E. *Photochem. Photobiol.* **1973**, *18*, 293–301.
- (35) Birge, R. R.; Schulten, K.; Karplus, M. *Chem. Phys. Lett.* **1975**, *31*, 451–454.
- (36) Birge, R.; Pierce, B. *J. Chem. Phys.* **1979**, *70*, 165–167.
- (37) Enriquez, M. M.; Fuciman, M.; LaFountain, A. M.; Wagner, N. L.; Birge, R. R.; Frank, H. A. *J. Phys. Chem. B* **2010**, *114*, 12416–12426.
- (38) Savitzky, A.; Golay, M. J. E. *Anal. Chem.* **1964**, *36*, 1627–1639.
- (39) Steinier, J.; Termonia, Y.; Deltour, J. *Anal. Chem.* **1972**, *44*, 1906–1909.
- (40) Lakowicz, J. R. *Principles of Fluorescence Spectroscopy*; 2nd ed.; Kluwer Academic, Plenum Publishers: New York, 1999.
- (41) Ilagan, R. P.; Christensen, R. L.; Chapp, T. W.; Gibson, G. N.; Pascher, T.; Polivka, T.; Frank, H. A. *J. Phys. Chem. A* **2005**, *109*, 3120–3127.
- (42) van Stokkum, I. H. M.; Larsen, D. S.; van Grondelle, R. *Biochim. Biophys. Acta* **2004**, *1657*, 82–104.
- (43) Martin, C. H.; Birge, R. R. *J. Phys. Chem. A* **1998**, *102*, 852–860.
- (44) Premvardhan, L.; Sandberg, D. J.; Fey, H.; Birge, R. R.; Buchel, C.; van Grondelle, R. *J. Phys. Chem. B* **2008**, *112*, 11838–11853.
- (45) Niedzwiedzki, D. M.; Sandberg, D. J.; Cong, H.; Sandberg, M. N.; Gibson, G. N.; Birge, R. R.; Frank, H. A. *Chem. Phys.* **2009**, *357*, 4–16.
- (46) Foresman, J. B.; Head-Gordon, M.; Pople, J. A.; Frisch, M. J. *J. Phys. Chem.* **1992**, *96*, 135–149.
- (47) Stanton, J. F.; Bartlett, R. J. *J. Chem. Phys.* **1993**, *98*, 7029–7039.
- (48) Koch, H.; Kobayashi, R.; Sánchez de Merás, A.; Jørgensen, P. *J. Chem. Phys.* **1994**, *100*, 4393–4400.
- (49) Kállay, M.; Gauss, J. *J. Chem. Phys.* **2004**, *121*, 9257–9269.
- (50) Nakajima, T.; Nakatsuji, H. *Chem. Phys.* **1999**, *242*, 177–193.
- (51) Ishida, M.; Toyota, K.; Ehara, M.; Frisch, M. J.; Nakatsuji, H. *J. Chem. Phys.* **2004**, *120*, 2593–2605.
- (52) Frisch, M. J.; Trucks, G. W.; Schlegel, H. B.; Scuseria, G. E.; Robb, M. A.; Cheeseman, J. R.; Scalmani, G.; Barone, V.; Mennucci, B.; Petersson, G. A.; et al. *Gaussian 09*, revision A.02; Gaussian, Inc.: Wallingford, CT, 2009.
- (53) Nakatsuji, H. *Chem. Phys. Lett.* **1978**, *59*, 362–364.
- (54) Krylov, A. I. *Annu. Rev. Phys. Chem.* **2008**, *59*, 433–462.
- (55) Head-Gordon, M.; Pople, J. A.; Frisch, M. J. *Chem. Phys. Lett.* **1988**, *153*, 503–506.
- (56) Dunning T. H., Jr.; Hay, P. J. In *Modern Theoretical Chemistry*; Schaefer, H. F., Ed.; Plenum: New York, 1976; Vol. 3, pp 1–28.
- (57) Niedzwiedzki, D.; Kosciielecki, J. F.; Cong, H.; Sullivan, J. O.; Gibson, G. N.; Birge, R. R.; Frank, H. A. *J. Phys. Chem. B* **2007**, *111*, 5984–5998.
- (58) Rondonuwu, F. S.; Watanabe, Y.; Fujii, R.; Koyama, Y. *Chem. Phys. Lett.* **2003**, *376*, 292–301.
- (59) Pendon, Z. D.; Gibson, G. N.; van der Hoef, I.; Lugtenburg, J.; Frank, H. A. *J. Phys. Chem. B* **2005**, *109*, 21172–21179.
- (60) Kosumi, D.; Yanagi, K.; Fujii, R.; Hashimoto, H.; Yoshizawa, M. *Chem. Phys. Lett.* **2006**, *425*, 66–70.
- (61) Billsten, H. H.; Zigmantas, D.; Sundström, V.; Polivka, T. *Chem. Phys. Lett.* **2002**, *355*, 465–470.
- (62) de Weerd, F. L.; van Stokkum, I. H. M.; van Grondelle, R. *Chem. Phys. Lett.* **2002**, *354*, 38–43.
- (63) Niedzwiedzki, D. M.; Sullivan, J. O.; Polivka, T.; Birge, R. R.; Frank, H. A. *J. Phys. Chem. B* **2006**, *110*, 22872–22885.
- (64) Frank, H. A.; Josue, J. S.; Bautista, J. A.; van der Hoef, I.; Jansen, F. J.; Lugtenburg, J.; Wiederrecht, G.; Christensen, R. L. *J. Phys. Chem. B* **2002**, *106*, 2083–2092.
- (65) Andersson, P. O.; Bachilo, S. M.; Chen, R.-L.; Gillbro, T. *J. Phys. Chem.* **1995**, *99*, 16199–16209.
- (66) Englman, R.; Jortner, J. *Mol. Phys.* **1970**, *18*, 145–164.
- (67) Papagiannakis, E.; van Stokkum, I. H.; Vengris, M.; Cogdell, R. J.; van Grondelle, R.; Larsen, D. S. *J. Phys. Chem. B* **2006**, *110*, 5727–5736.
- (68) Larsen, D. S.; Papagiannakis, E.; van Stokkum, I. H. M.; Vengris, M.; Kennis, J. T. M.; van Grondelle, R. *Chem. Phys. Lett.* **2003**, *381*, 733–742.
- (69) Wohlleben, W.; Buckup, T.; Hashimoto, H.; Cogdell, R. J.; Herek, J. L.; Motzkus, M. *J. Phys. Chem. B* **2004**, *108*, 3320–3325.
- (70) Billsten, H. H.; Pan, J.; Sinha, S.; Pascher, T.; Sundström, V.; Polivka, T. *J. Phys. Chem. A* **2005**, *109*, 6852–6859.
- (71) Polivka, T.; Sundström, V. *Chem. Phys. Lett.* **2009**, *477*, 1–11.
- (72) Jailaubekov, A. E.; Song, S.-H.; Vengris, M.; Cogdell, R. J.; Larsen, D. S. *Chem. Phys. Lett.* **2010**, *487*, 101–107.
- (73) Lenzer, T.; Ehlers, F.; Scholz, M.; Oswald, R.; Oum, K. *Phys. Chem. Chem. Phys.* **2010**, *12*, 8832–8839.
- (74) Calhoun, T. R.; Davis, J. A.; Graham, M. W.; Fleming, G. R. *Chem. Phys. Lett.* **2012**, *523*, 1–5.
- (75) Bilotti, K. The Thermal and Photochemical Stabilities and the Excited Electronic States of Natural and Synthetic Polyenes. Bowdoin College, 2010.
- (76) Gradinaru, C. C.; Kennis, J. T. M.; Papagiannakis, E.; van Stokkum, I. H. M.; Cogdell, R. J.; Fleming, G. R.; Niederman, R. A.; van Grondelle, R. *Proc. Natl. Acad. Sci. U.S.A.* **2001**, *98*, 2364–2369.
- (77) Chábera, P.; Fuciman, M.; Hřibek, P.; Polivka, T. *Phys. Chem. Chem. Phys.* **2009**, *11*, 8795–8803.
- (78) Ostroumov, E. E.; Müller, M. G.; Reus, M.; Holzwarth, A. R. *J. Phys. Chem. A* **2011**, *115*, 3698–3712.
- (79) Papagiannakis, E.; van Stokkum, I. H. M.; van Grondelle, R. *J. Phys. Chem. B* **2003**, *107*, 11216–11223.
- (80) Christensen, R. L.; Barney, E. A.; Broene, R. D.; Galinato, M. G. I.; Frank, H. A. *Arch. Biochem. Biophys.* **2004**, *430*, 30–36.
- (81) Galinato, M. G. I. Optical Spectroscopic Studies of Simple Polyenes and Complex Xanthophylls. Ph.D. Dissertation, University of Connecticut, 2007.
- (82) Christensen, R. L.; Goyette, M.; Gallagher, L.; Duncan, J.; DeCoster, B.; Lugtenburg, J.; Jansen, F. J.; van der Hoef, I. *J. Phys. Chem. A* **1999**, *103*, 2399–2407.
- (83) Schaffer, H. E.; Chance, R. R.; Silbey, R. J.; Knoll, K.; Schrock, R. R. *J. Chem. Phys.* **1991**, *94*, 4161–4170.
- (84) Caricato, M.; Mennucci, B.; Scalmani, G.; Trucks, G. W.; Frisch, M. J. *J. Chem. Phys.* **2010**, *132*, 084102.
- (85) Fukuda, R.; Ehara, M.; Nakatsuji, H.; Cammi, R. *J. Chem. Phys.* **2011**, *134*, 104109.
- (86) Marenich, A. V.; Cramer, C. J.; Truhlar, D. G.; Guido, C. A.; Mennucci, B.; Scalmani, G.; Frisch, M. J. *Chem. Sci.* **2011**, *2*, 2143–2161.
- (87) Zechmeister, L. *Cis-Trans Isomeric Carotenoids, Vitamin A, and Arylpolyenes*; Academic Press: New York, 1962.
- (88) Honig, B.; Dinur, U.; Birge, R. R.; Ebrey, T. G. *J. Am. Chem. Soc.* **1980**, *102*, 488–494.
- (89) Tavan, P.; Schulten, K. *Phys. Rev. B: Condens. Matter* **1987**, *36*, 4337–4358.
- (90) Schmidt, M.; Tavan, P. *J. Chem. Phys.* **2012**, *136*, 124309.
- (91) Koyama, Y.; Rondonuwu, F. S.; Fujii, R.; Watanabe, Y. *Biopolymers* **2004**, *74*, 2–18.
- (92) Koyama, Y.; Kakitani, Y.; Miki, T.; Christiana, R.; Nagae, H. *Int. J. Mol. Sci.* **2010**, *11*, 1888–1929.
- (93) Christensen, R. L.; Faksh, A.; Meyers, J. A.; Samuel, I. D. W.; Wood, P.; Schrock, R. R.; Hultsch, K. C. *J. Phys. Chem. A* **2004**, *108*, 8229–8236.
- (94) Fuss, W.; Haas, Y.; Zilberg, S. *Chem. Phys.* **2000**, *259*, 273–295.

- (95) Garavelli, M.; Celani, P.; Fato, M.; Bearpark, M. J.; Smith, B. R.; Olivucci, M.; Robb, M. A. *J. Phys. Chem. A* **1997**, *101*, 2023–2032.
- (96) Fuss, W.; Lochbrunner, S.; Müller, A.; Schikarski, T.; Schmid, W.; Trushin, S. *Chem. Phys.* **1998**, *232*, 161–174.
- (97) Antognazza, M. R.; Lüer, L.; Polli, D.; Christensen, R. L.; Schrock, R. R.; Lanzani, G.; Cerullo, G. *Chem. Phys.* **2010**, *373*, 115–121.
- (98) Billstein, H. H.; Herek, J. L.; Garcia-Asua, G.; Hashoj, L.; Hunter, C. N.; Sundström, V. *Biochemistry* **2002**, *41*, 4127–4136.
- (99) Wasielewski, M. R.; Johnson, D. G.; Bradford, E. G.; Kispert, L. D. *J. Chem. Phys.* **1989**, *91*, 6691–6697.